Energy Conversion and Management 282 (2023) 116811

Contents lists available at ScienceDirect

Energy Conversion and Management

journal homepage: www.elsevier.com/locate/enconman

Reliable control of turbine–generator set for oscillating-water-column wave energy converters: Numerical modelling and field data comparison

A.A.D. Carrelhas, L.M.C. Gato *

IDMEC, Instituto Superior Técnico, Universidade de Lisboa, Av. Rovisco Pais 1, 1049-001 Lisboa, Portugal

ARTICLE INFO

Keywords:
Wave energy
Oscillating water column
Air turbine
PTO control
Numerical modelling
Field data comparison

ABSTRACT

Global energy strategy has quickly shifted to a new paradigm. Countries understand the importance of a near-zero carbon energy mix and the need to reduce their energy imports and become energy independent. One immediate solution is the re-enforcement of renewable energy infrastructures such as wind, solar and hydro generation. However, certain sectors, particularly the Blue Economy, may need a different solution. The oscillating-water-column (OWC) wave energy converter is a proven concept, many prototypes of which are already being deployed on the open sea, and can help bridge this gap. Energy harvesting from this system will be improved if more efficient (and reliable) power take-off (PTO) systems and control algorithms are used. A novel control algorithm for a turbine–generator set was developed based on the physical interactions between the PTO and the OWC system. The results were compared with experimental data from real operation at sea. The algorithm does not need to predict the sea state conditions in order to maximise power generation. Additionally, it protects the PTO in extremely energetic sea states and minimises overspeeding and the use of a safety valve. Comparing the operating results of the 30 kW biradial turbine–generator set at the Mutriku wave power plant with the corresponding numerical results provided by the novel control algorithm showed a 6% increase in annual electricity production.

1. Introduction

The world is at the dawn of a new energy paradigm. From the findings of the Intergovernmental Panel on Climate Change (IPCC) [1] to the growing fear of reaching climate tipping points [2], once considered far-fetched, the focus is now clear: the transition to a zero-carbon, high-efficiency energy sector [3], also called the energy transition. Strong policies [4] have used funds, taxes and subsidies [5] to enable the necessary gradual transformation of the current energy mix [6] from markets with a high share of conventional polluting energy resources to a near zero-carbon market with a high penetration of renewable energy resource technologies [7,8]. Moreover, this dynamic means that energy demand will increase as it is expected to electrify everyday products and various sectors [9]. Thus, to keep energy prices affordable, supply must increase.

Although wind, solar and hydropower are likely to be the leading renewable energy technologies to meet energy needs [10], there are certain situations where their role is less appropriate and other technologies, such as renewable marine energy, provide an excellent solution [11,12]. Namely, engaging in solutions to sustain Blue Economy (e.g.: aquaculture [13], decarbonisation of ports [14], oceanographic monitoring [15,16] or small coastal communities [17]).

Offshore wind energy technologies are experiencing rapid growth, with an new installed capacity of nearly 29 GW in 2019 and an estimated increase to 35 times in 2050 [18]. Due to bathymetry issues in some potential markets, such as the United States and Japan, which have few shallow-water sites, this technology is expected to be used more in deep waters [19]. Therefore, floating foundations are to be used and an installed capacity of up to 150 GW is envisaged by 2050 [18]. The potential for large turbines of up to 20 MW [18] has led to a large amount of funding being poured into this technology, making it probably the biggest threat to the development and funding of wave energy converters (WECs). The introduction of this new technology has set a new level of cost that wave energy technologies must reach if they are to compete in the renewable energy market. Like the offshore wind industry, wave energy technologies can use the accumulated knowledge from the oil and gas industry to develop and consolidate improved concepts for the structural foundations, operation and maintenance of WECs [20].

A common unfair analysis directly compares the energy extracted from a single WEC and a single wind turbine. This comparison devalues WECs because the amount of energy extracted from each converter is inherently limited. It also does not consider the array effect [21,22],

* Corresponding author.
E-mail addresses: ana.carrelhas@tecnico.ulisboa.pt (A.A.D. Carrelhas), luis.gato@tecnico.ulisboa.pt (L.M.C. Gato).

https://doi.org/10.1016/j.enconman.2023.116811
Received 24 November 2022; Received in revised form 22 January 2023; Accepted 10 February 2023
Available online 8 March 2023

Nomenclature

Romans

a	Control law parameter [Nm s^b]
b	Control law parameter
D	Rotor diameter [m]
f_o	Frequency of occurrence
F	Fitness function
H_s	Significant wave height [m]
I	Inertia [kg m^2]
K	Constant of Eq. (5)
MAEP	Mean annual electricity production [Wh]
p	Pressure [Pa]
P	Power [W]
Q	Flow rate [m^3/s]
t	Time [s]
T	Torque [Nm]
T_p	Peak period [s]

Greek symbols

Δ	Variation, interval
Δp	Turbine available pressure head [Pa]
η	Efficiency
Π	Power coefficient
ρ	Fluid density [kg/m^3]
Φ	Flow coefficient
Ψ	Pressure coefficient
Ω	Rotational speed [rad/s]

Superscripts

$*$	Dimensionless value
$-$	Average quantity
i	Sea state index
lim	Limit
rated	Rated quantity
ref	Reference
RO	Regular operation
SM	Safe-mode operation

Subscripts

avail	Available
bep	Best efficiency point
CL	Control law
elec	Electrical
f	Final
gen	Generator
i	Initial
j	Test number
L	Lower-threshold
max	Maximum
RO	Regular operation
rated	Rated quantity
Thrs	Threshold
total	Total
turb	Turbine
U	Upper-threshold

Acronyms

BCA	Best Control Algorithm
CAPEX	Capital Expenditures
ga	Genetic Algorithm
H2020	Horizon 2020
IST	Instituto Superior Técnico
IPCC	Intergovernmental Panel on Climate Change
OPERA	Open Sea Operating Experience to Reduce Wave Energy Cost
OPEX	Operational Expenditure
OWC	Oscillating Water Column
PLC	Programmable Logic Controller
PTO	Power Take-off System
RO	Regular Operation
SM	Safe Mode
WEC	Wave Energy Converter

which can be used to increase the system's overall efficiency, nor the cost of construction, installation, maintenance, space requirements or separation between devices. The challenge for the next generation of WECs is to develop simple and reliable devices with minimal maintenance costs that compete with rapidly emerging offshore wind technologies. It is necessary to install as many devices as possible to achieve CAPEX and OPEX values that the market can absorb. To achieve this goal, research communities, companies and governments must make a concurrent effort to promote the construction and testing of many prototypes under real ocean conditions. Testing should be carried out in the first phase in open test facilities such as EMEC (Scotland), Galway Bay (Ireland), Belmullet (Ireland), BiMEP (Spain), Mutriku (Spain) or Viana do Castelo (Portugal) to gain further experience in critical areas such as operation and maintenance, installation, commissioning and decommissioning. Fundamental steps such as those mentioned increase the technological readiness and reduce the risk of the sector, but also promote the necessary steps towards licencing, legislation and a smooth transition to introduce wave energy into the energy mix [23] as has been the case with solar and wind technologies, which have been continuously invested in, researched, developed and deployed over the last 30 years.

The oscillating water column (OWC) is a proven WEC concept [24] with many prototypes deployed in the open ocean. There are fixed [25,26] and floating structures [27]. The floating type has similarities with offshore wind technologies, e.g., floaters, moorings, electronic components and manufacturing processes. The power take-off systems (PTO) that equip these units are turbine–generator sets [28], with Wells [29] and impulse turbines [30] being the most popular choice. The energy extraction from OWC WECs will improve as more efficient (and reliable) PTOs become available along with advanced control algorithms [31].

Most of the control strategies published in recent years are mainly related to non-OWC WEC types [32]. Those studying OWC systems usually focus on one or two of their subcomponents to maximise electricity production: (i) the hydrodynamics of the device, (ii) the air turbine, and (iii) the electric generator. Most numerical models consider a PTO whose turbine is of the Wells [33,34] type. The Wells turbine is a relatively low-cost option due to its simple construction. However, it has a narrow operating range compared to impulse turbines due to stall on the rotor blades above a certain flow rate threshold [35], which can affect the cost of electricity of the system. Due to their specific operating characteristics, the two types of turbines cannot use the same control algorithm strategy. There is less published work for impulse turbines than for Wells turbines [36]. Most impulse turbine control algorithms have been developed for axial-flow turbines [37].

Only a few papers deal with the joint study of the behaviour of air turbines and generators under different sea state conditions [38,39]. There are two possible explanations for this: (i) either the authors choose an "off-the-shelf" turbine with some design features and proceed with the development of the control algorithms, or (ii) the turbine designers have a sound knowledge of the fluid dynamics in the whole turbomachine, but not of the control strategies of the whole WEC. Both situations are plausible (and understandable) as they are completely different technical problems. However, in resonant WECs, such as the OWC type, the control of the PTO can affect both the PTO efficiency and the hydrodynamic efficiency (conversion of energy from the waves), depending on the air turbine used. Consequently, the control of the PTO of the OWC device depends on a comprehensive understanding of the overall system, and the control algorithm should be designed to be coupled with the physics of the WEC.

In addition, real-world experience provides a macro view of the needs. Thus, the integration of the algorithm into the industrial control equipment, i.e. the programmable logic controller (PLC), the minimisation of the sensors used, the caution of the sensors used due to problems in the field, such as introducing noise into the input/output signals or delays in the sensors/actuators, and the effects of fatigue on the components of the system must be considered.

Several OWC PTOs have already been tested in real sea conditions, such as in (i) the Pico plant [40], (ii) the Limpet [41], (iii) the OE buoy [42] and (iv) the Oceanlinx MK3 [43]. As is to be expected with new technology, the main focus of the first deployments is to ensure that the device can be commissioned and operated safely and withstand real ocean conditions during the test campaign. In most cases, the lessons learnt remain with the developer for commercial reasons, so the knowledge gained is not disseminated throughout the research and development community. In contrast, the European H2020 project OPERA [44] published data from more than a year of operation of the biradial air turbine [45] at the Mutriku wave power plant. It provided a unique opportunity to explore the results of an experimental campaign under real conditions, learn from them and develop new solutions to increase the maturity of the wave energy sector.

The OPERA project was a 5-year project in which the novel biradial air turbine for OWC applications was built and tested in three different environments: (i) under controlled conditions at the IST 55 kW Variable Flow Laboratory [46,47]; (ii) at the Mutriku wave power plant [48] and; (iii) at the BiMEP test site, installed in IDOM's MARMOK-A5 device [49].

The test results of OPERA's project trial campaign at the Mutriku facility are reported in Refs. [50,51]. These include non-adaptive and adaptive control laws based on one or more variables from rotational speed, pressure in the pneumatic chamber, electric generator power output, hourly sea state data, next wave information, high-speed valve shutter position and OWC motion as reported in Refs. [50,51] and summarised in Table 1. The control laws tested worked alternatively, allowing comparison between the control laws for the prevailing sea state and tuning of the control law parameters [50,51]. The OPERA's tests at the Mutriku facility aimed to experiment with various control algorithms, and consequently, several non-optimal parameterisations were tested [50,51]. Some problems contributed to the non-optimal control of the turbine–generator set, such as open-loop control and a misconception of the self-starting capabilities of the biradial turbine operation [50,51].

The subject of this paper is the control of the biradial air turbine, for which few studies of control algorithms are available. Some focus on numerical simulations [52–55], others involve experimental validation [56], but most of them were produced in the framework of the OPERA project [39,50,51,57,58]. This paper presents and analyses a novel control algorithm for the turbine–generator set that could have been used during the experimental campaign of the OPERA project. The design of the control algorithm described in this paper is based on the analysis of the results and lessons learnt from the project OPERA. The algorithm represents a new approach to control OWC devices, as the physics of the air turbine installed in an OWC is used for its development. The measurement of the rotational speed and the pneumatic chamber pressure are the only inputs for the proposed control of the torque of the generator. It is thus an evolution of the CL1 control law of the OPERA project [51] (Table 1), designed to maximise the power output of the PTO when its operation is safe and to use the time-averaged available pneumatic power of the turbine over a backward time horizon to switch to a safe operating mode when needed. Unlike some existing control algorithms [50,51,57], prediction of sea state conditions is not required, so data from a real-time wave measurement system near the OWC device is not needed, which has proven to be quite difficult and fraught with uncertainty [51]. It is also very reliable as it minimises the operation of a safety valve. The experimental data recorded during the experimental campaign are available in the public Zenodo database [59] and are used as input to the numerical model that replicates the performance of the turbine–generator set in the Mutriku wave power plant. Comparing the numerical data of the new control algorithm with the experimental data from the project OPERA has validated the new algorithm and shown its good performance for future industrial applications.

Table 1
Summary of the OPERA's control laws for the biradial turbine.
Source: Adapted from [51].

Law	Control	Input
CL1	Generator torque	Rotational speed
CL2	Generator torque	Chamber pressure
CL3	PTO damping, valve open-close timings	Hourly sea-state data
CL4	Valve open-close timings and shutter position	Rotational speed, chamber pressure and valve shutter position
CL5	Generator torque	Next wave information, rotational speed and generator power output
CL6	Generator torque	OWC motion, chamber pressure, rotational speed and wave elevation

The research question to be answered in this paper is: Can a control algorithm be developed that maximises energy output without knowledge of sea state conditions, and that can be integrated into reliable and simple industrial equipment?

The main contributions of the current work are:

1. Critical analysis of data obtained during an experimental campaign under real sea state conditions and direct application of the knowledge gained to develop a new control strategy for turbine–generator sets for OWC WECs.
2. Development of a control algorithm for a biradial air turbine.
3. Development of a novel control algorithm based on the system physics of OWC WECs to enable safe and reliable operation.
4. An in-depth and comprehensive analysis of the results carefully describes the performance of the air turbine and the electric generator.
5. Comparison of the numerical results with real operation data measured at the Mutriku wave power plant.

The structure of the paper is as follows. The PTO system under study is described in Section 2. Then, in Section 3, the method used to develop the novel control algorithm is presented. The analysis of the results and the conclusions are presented in Sections 4 and 5, respectively.

2. Power take-off system

The Mutriku power plant consists of sixteen pneumatic chambers with a width of 4.5 m, a length of 4.3 m and a height of 7.45 m above the highest equinoctial spring tide. It has been integrated into the 440 m long local breakwater since 2011 [60], see Fig. 1 a). The Wells turbines, rated at 18.5 kW, are connected at the top of each pneumatic chamber within a common gallery. The biradial turbine

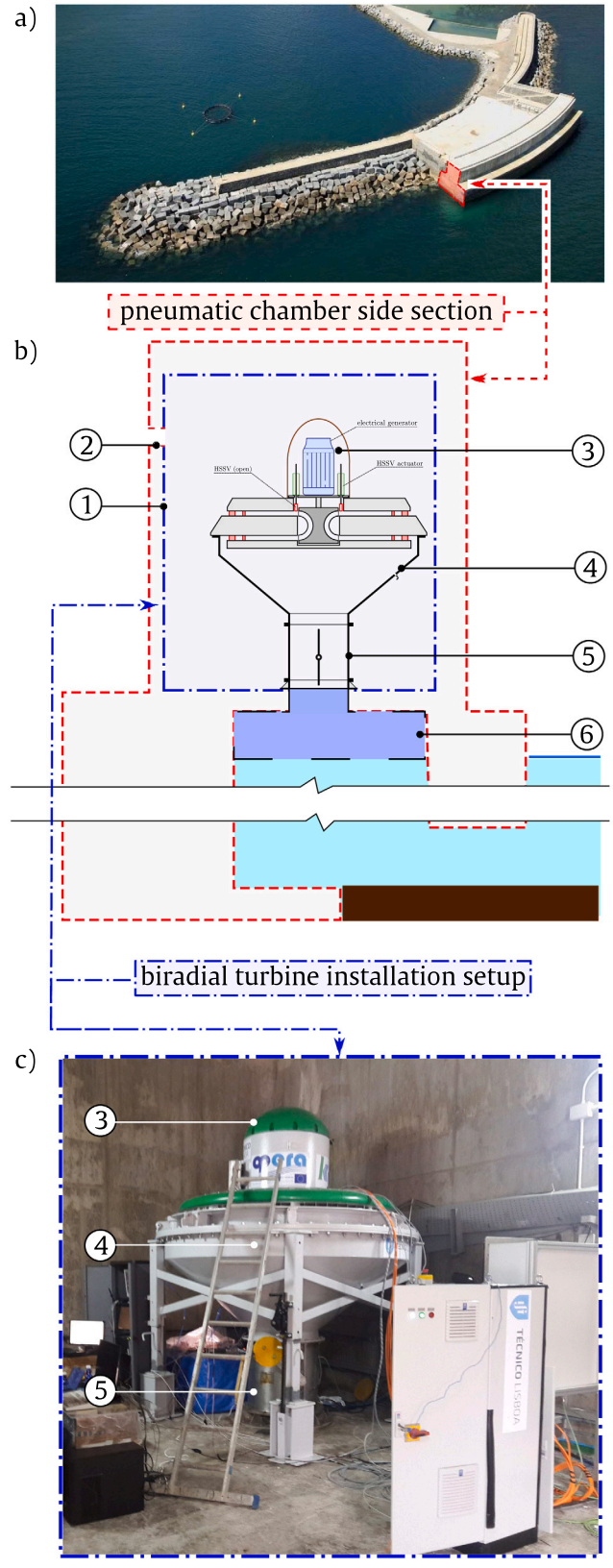

Fig. 1. Mutriku's wave power plant: (a) Bird's eye view of the plant; (b) Side section schematic view of one pneumatic chamber, adapted from [48] (not to scale, the height is considerably larger when compared with the width [60]); (c) Photograph of the turbine's gallery. 1 - Turbine's gallery; 2 - Opening to the atmosphere; 3 - PTO; 4 - Conical adapter; 5 - Interface duct with the power plant butterfly valve; 6 - Pneumatic chamber.

Table 2
Power take-off system main characteristics.
Source: Reproduced from Ref. [47].

WEC type	fixed OWC
Air turbine	biradial turbine
Assembly position	vertical axis
Rated power, $P_{\text{gen}}^{\text{rated}}$ [kW]	30
Maximum speed, Ω_{max} [rad/s]	314
Maximum generator counter torque, $T_{\text{gen}}^{\text{lim}}$ [Nm]	256
Turbine rotor diameter D [m]	0.50
Turbine stator diameter [m]	2.10
Distributor type	4×64 fixed guide vanes
Safety valve	high-speed
Turbine rotor inertia, I [kg m^2]	5.01

from the OPERA project was mounted in chamber nine via a conical adapter, see Fig. 1 b) and c).

The PTO system consists of a biradial air turbine with a new stator design [45,61], a 30 kW electric generator and a high-speed safety valve, see Fig. 1 c). The built-in high-speed safety valve is located on the atmosphere side of the turbine stator, close to the rotor [47]. It is axially movable and allows no and partial to complete blockage of the flow by means of linear actuators. Table 2 contains additional information about the turbine and generator. For more details on the turbine–generator set components and the turbine aerodynamic design strategy, see Refs. [45,47]. The PTO was installed at the Mutriku wave power plant to be tested between May 2017 and June 2018. In the first phase, from May to June 2017, the team from IST was the consortium partner that carried out the commissioning tests. In the second phase, from June 2017 to June 2018, the consortium tested six advanced control algorithms. The field data from this phase is available online [59]. Measurements of rotational speed, turbine pressure head, output power, water column motion in the chamber and wave height upstream of the plant were used for the adaptive and predictive control laws implemented and tested [50,62].

At high Reynolds numbers and low Mach numbers, the performance characteristics of the turbine are described in dimensionless form by the turbine pressure head coefficient [63],

$$\Psi = \frac{\Delta p}{\rho \Omega^2 D^2}, \tag{1}$$

the flow rate coefficient,

$$\Phi = \frac{Q}{\Omega D^3}, \tag{2}$$

the power coefficient,

$$\Pi = \frac{T_{\text{turb}}}{\rho \Omega^2 D^5}, \tag{3}$$

and the efficiency,

$$\eta_{\text{turb}} = \frac{\Pi}{\Phi \Psi}, \tag{4}$$

as presented in Fig. 2. Here, Q is the volumetric flow rate, D is the turbine rotor diameter, Ω is the rotational speed, ρ is the air density at the turbine inlet, Δp is the turbine pressure head and T_{turb} is the turbine shaft torque. The experimental results of Ref. [47] are shown in black circles in Fig. 2. The coloured lines are the curves resulting from the data fitting used in this work.

The electric generator is a standard squirrel-cage induction machine with a rated output of $P_{\text{gen}}^{\text{rated}} = 30$ kW, operating in four quadrants. Before installation in the turbine, the efficiency of the generator was determined experimentally as a function of the rotational speed and load. The results are shown in Fig. 3.

3. Method

A flowchart of the method used to develop the control algorithm is shown in Fig. 4. The method is as follows:

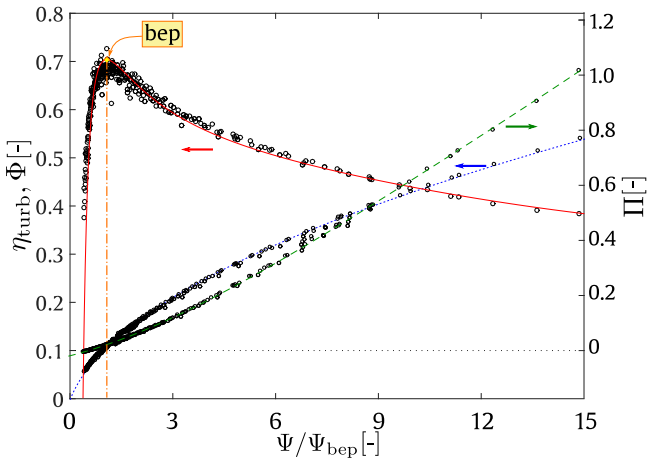

Fig. 2. Efficiency (η_{turb}), flow (Φ) and power coefficients (Π) as a function of the turbine pressure head coefficient (Ψ). Experimental results: black circles [47]. Fittings: η_{turb} - red line; Φ - blue line; Π - green line. Best efficiency point (bep): $\Psi_{bep} = 0.360$, $\Pi_{bep} = 0.0290$ and $\Phi_{bep} = 0.115$.

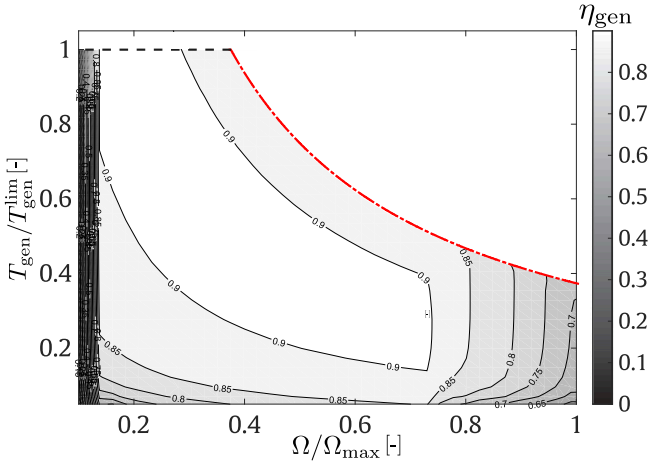

Fig. 3. Generator efficiency map [47]. The maximum generator counter torque is represented by the colour lines: dotted blue line - $T_{gen}^{lim}/T_{gen}^{lim}$; dot-dashed red line - $P_{rated}/(\Omega T_{gen}^{lim})$.

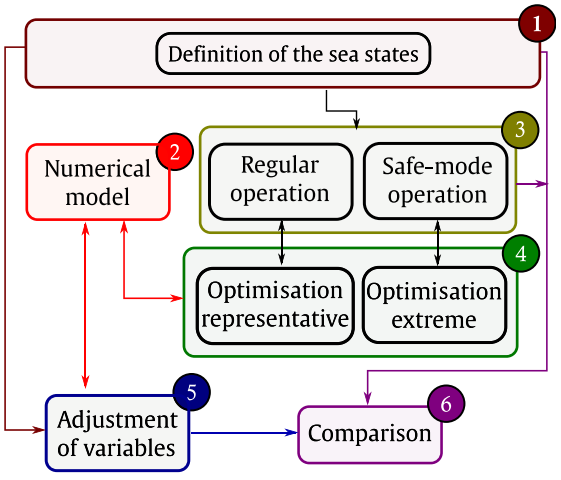

Fig. 4. Method flowchart: 1 - Definition of the sea states; 2 - Numerical model; 3 - Control algorithm strategy; 4 - Optimisation; 5 - Adjustment of variables; 6 - Comparison.

1. Definition of sea states: The data available in the Zenodo database from the experimental campaign of the biradial turbine of the OPERA project at the Mutriku wave power plant are compared with the local hourly data of sea state conditions at the SIMAR point 3171032 [64]. The aim is to identify the sea state conditions for each test in the Zenodo database; see Section 3.1.
2. Numerical model: A numerical model reproduces the behaviour of OPERA's 30 kW turbine–generator set at Mutriku wave power plant, see Section 3.2.
3. Control algorithm: A novel control strategy based on the rotational speed and time-averaged available pneumatic power of the turbine over a backward time horizon is used to maximise electricity production. This strategy uses two operating modes: regular mode and safe mode, see Section 3.3.
4. Optimisation algorithm: A genetic algorithm explores and finds the best variables for implementing the control algorithm's regular and safe operation modes. At the same time, it satisfies the imposed constraints and minimises the proposed objective functions; see Section 3.4.
5. Adjustment of variables: Some test variables from the database had to be adjusted to fairly compare the results of the experimental campaign from the project OPERA with those of the current study, see Section 3.5.
6. Comparison of results: The results of the numerical simulations are compared with real data from the experimental campaign at the Mutriku wave power plant.

3.1. Definition of the sea states

The data from the experimental campaigns at the Mutriku wave power plant are available online in the Zenodo database [59]. There are 257 test results from almost a year of testing, from June 2017 to June 2018. For each test, the dataset contains time series of relevant data related to turbine and generator operation (see Appendix A). The database contains the hour and date of each test, but not two essential variables to characterise the sea state conditions: the significant height H_s, and the peak period, T_p.

Wave data from oceanographic buoys in the coastal areas of Spain are available in the database *Puertos del Estado* [64]. Among other variables, this database contains information on the significant wave height H_s, the peak period T_p, and the corresponding frequency of occurrence f_o, obtained from measurements of up to 60 years. For each oceanographic buoy location, the wave climate is defined by a frequency of occurrence matrix of sea states resulting from the discretisation of H_s and T_p at intervals of 0.5 m and 2 s, respectively. The buoy closest to the Mutriku wave power plant is at SIMAR point 3171032 (see Ref. [64]), and its measurements were used to estimate the H_s and T_p corresponding to each test available in the Zenodo database.

Fig. 5 a) shows the frequency of occurrence for each bin of H_s and T_p. The bin discretisation is shown in the *Puertos del Estado* database. Fig. 5 b) presents the number of tests from the Zenodo database contained in each bin. It can be seen that the available tests are not evenly distributed among the different bins. From Fig. 5 a) it can be seen that the sum of all frequencies of the Zenodo database bins is 95.2%, and these cases correspond to 80% of the total available pneumatic power. Therefore, the results in this database can be considered fairly representative of the local wave energy resource. For each bin with at least one test, an index was defined to facilitate further analysis of the results (see Fig. 5 c)). A total of 27 sea states were defined.

A detailed analysis of the time series of the turbine pressure head for the sea states defined above shows that while the root-mean-square of the pressure head is similar between tests in the same bin, significant differences are observed between the maximum and minimum values of the time series. Therefore, two subsets of 27 sea states were identified as representative and extreme. Representative and extreme are tests that describe the average and extreme conditions of the test set of

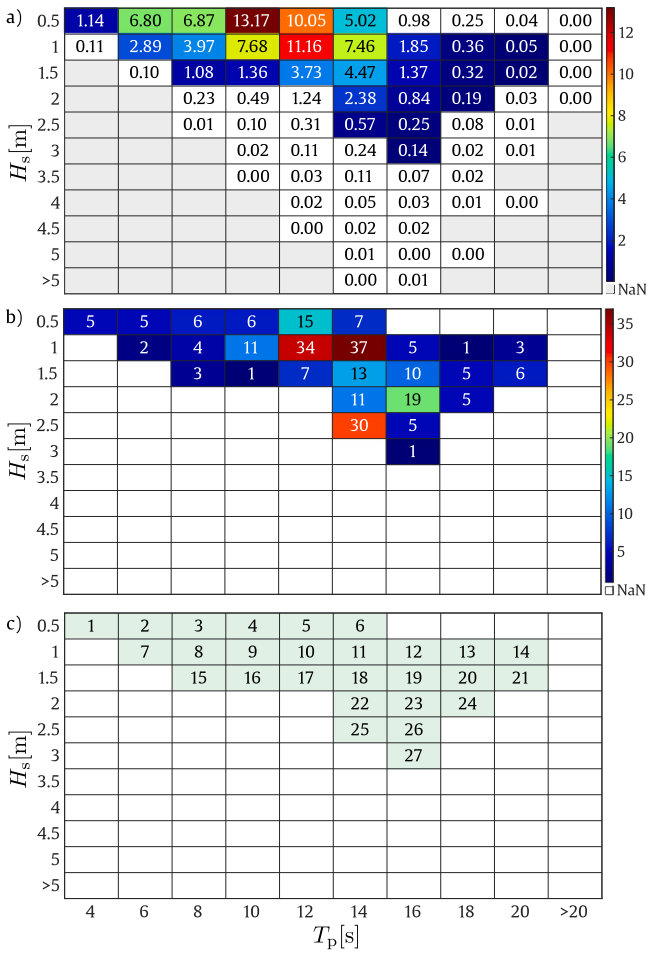

Fig. 5. Definition of sea states: a) Frequency of occurrence f_o in % (white colour indicates bins with no data); b) Number of tests in the Zenodo's database for each (H_s, T_p) bin and; c) Sea state index for each bin with available data.

a particular bin. For example, there are 34 tests for $H_s = 1$ m and $T_p = 12$ s, see Fig. 5 b). Of these 34 tests, those that present characteristics closer (distant with higher energy) to the average conditions go to the representative (extreme) sub-set.

3.2. Numerical model

A numerical model was developed to replicate the behaviour of the biradial air turbine of the OPERA project at the Mutriku wave power plant. Typically, a numerical wave-to-wire model of an OWC WEC is as follows [65,66]. An incident wave characterised by H_s and T_p causes the water-free surface of the OWC to move within the pneumatic chamber. The corresponding time-dependent pressure variation generates a flow rate through an air turbine. The turbine converts the available pneumatic power into shaft power, which drives an electric generator. The turbine's rotational speed is a function of the instantaneous available pneumatic power and the counter torque of the generator. In general, the turbine rotational speed changes the turbine damping (ratio between turbine flow rate and turbine pressure head), which affects the hydrodynamic process of energy conversion. This is not the case with the biradial turbine, where the rotational speed has a negligible influence on the flow rate [47,67,68]. It is $\Psi(\Phi) \approx K\Phi^2$, where K is a constant. Then

$$\Delta p \approx \left(\frac{\rho K}{D^4}\right) Q^2 \,, \tag{5}$$

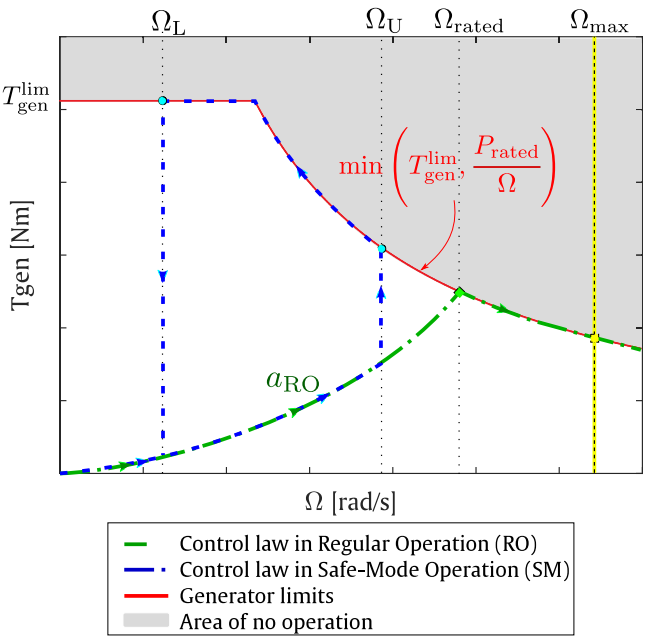

Fig. 6. Control algorithm strategy for regular operation and safe-mode operation.

which means that the turbine pressure head, in relation to the flow rate, does not depend on the turbine's rotational speed. This feature is crucial as it ensures that the control of the turbine–generator set does not affect the hydrodynamic energy conversion process for a given turbine geometry and size (damping). Consequently, using the time series of turbine pressure heads available in the Zenodo database for each sea state is valid and accurate for performing the numerical simulations presented in this paper, even if other control laws are used.

The former is the case when the high-speed safety valve of the turbine and the plant's butterfly valve are always fully open. Including the opening control of a valve connected in series or parallel in a control algorithm necessarily requires modelling the hydrodynamic process due to the effect of the damping variation in the dynamics of the pneumatic chamber introduced by the variation of the valve opening.

The differential equation governing the dynamics of the turbine–generator set is derived from Newton's second law of motion as

$$I\frac{\mathrm{d}\Omega(t)}{\mathrm{d}t} = T_{\mathrm{turb}}(t) - T_{\mathrm{gen}}(t)\,, \tag{6}$$

where I is the inertia of the rotating masses of the PTO (turbine, generator and other rotating subcomponents), t is time, and T_{gen} is the counter torque of the generator.

The finite difference method with backward differences approximates the first-order differential Eq. (6). Taking into account the turbine torque and the counter torque of the generator, the inertia and the rotational speed at time $t(n)$, the rotational speed at time $t(n+1)$ is then given by

$$\Omega(t+1) = \Omega(t) + \frac{\Delta t}{I}\Big(T_{\mathrm{turb}}(t) - T_{\mathrm{gen}}(t)\Big)\,, \tag{7}$$

where $\Delta t = t(n+1) - t(n)$ is the sampling time. The sampling time of the available time series is less than 0.25 s, which makes the error of the discretisation process introduced by Eq. (7) negligible.

3.3. Control strategy

The control algorithm is represented schematically in Fig. 6. There are two operating modes: (1) regular operation mode (RO) and (2) safe mode (SM).

The control law RO is based on the evidence that maximum power output is achieved with an ideal electric generator with constant efficiency and zero inertia turbine–generator set whose instantaneous rotational speed is controlled so that [38]

$$T_{\text{gen}}(t) = a_{\text{bep}}\Omega^2(t)\,. \tag{8}$$

Here $a_{\text{bep}} = \rho\Pi_{\text{bep}}D^5$ is the control parameter, where Π_{bep} is the value of the turbine power coefficient at the maximum efficiency point (best efficiency point (bep), see Fig. 2). It is assumed that ρ has negligible variation. In practice, a more general control law of the type

$$T_{\text{gen}} = a\Omega^b\,, \tag{9}$$

is used, where the values of the constants a and b maximise the electric generator power output, taking into account the inertia of the rotating masses and the effect of the efficiency of the electric generator [47]. Ref. [39] presents a sensitivity analysis of the control parameters a and b for rotational speed control of Wells and the biradial turbine. The results in Ref. [39] are plotted on a semi-logarithmic scale and show that both turbine–generator sets can operate at maximum efficiency over a wide range of control parameter pairs (a, b), which are determined by

$$b = b_{\text{ref}} + m\left(\ln a - \ln a_{\text{ref}}\right)\,, \tag{10}$$

where m is a constant that depends on the turbine–generator set, and $(a_{\text{ref}}, b_{\text{ref}})$ is a pair of reference control parameters chosen at a maximum efficiency point. Therefore, the control parameter b can be fixed without loss of generality. According to Eq. (8), $b = 2$ is assumed.

Based on the above, the control law during RO is defined as follows

$$T_{\text{gen}}^{\text{RO}} = \min\left(a_{\text{RO}}(\text{rms}(\Omega))\Omega^2,\ P_{\text{gen}}^{\text{rated}}/\Omega,\ T_{\text{gen}}^{\text{lim}}\right)\,, \tag{11}$$

where the control law parameter a_{RO} is a function of the root-mean-square of the rotational speed, rms(Ω), during a certain time interval to be determined, and $T_{\text{gen}}^{\text{lim}}$ is the maximum counter torque that the generator can apply, see Table 2. The control law follows the green dot-dashed line in Fig. 6.

The control algorithm goes into SM operation when:

1. the mean available pneumatic power, $\overline{P}_{\text{avail}}$, during a given time interval, Δt_{CL}, is larger than a given threshold value P_{thrs} and;
2. the instantaneous rotational speed is larger than a given upper-threshold value, $\Omega(t) > \Omega_{\text{U}}$.

The mean available pneumatic power is,

$$\overline{P}_{\text{avail}} = \frac{1}{t_{\text{f}} - t_{\text{i}}}\int_{t_{\text{i}}}^{t_{\text{f}}} Q(t)\Delta p(t)\text{d}t\,, \tag{12}$$

where t_{i} and t_{f} are the initial and final evaluation times. Under SM operation, the control law is

$$T_{\text{gen}}^{\text{SM}} = T_{\text{gen}}^{\text{max}}(\Omega) = \min\left(P_{\text{gen}}^{\text{rated}}/\Omega, T_{\text{gen}}^{\text{lim}}\right)\,. \tag{13}$$

Eq. (13) represents the maximum allowable counter torque the electric generator may apply. Therefore, the control follows the blue dot-dashed line in Fig. 6.

The control algorithm switches to RO when the instantaneous rotational speed is lower than a lower threshold, Ω_{L}, and the mean available pneumatic power, $\overline{P}_{\text{avail}}$, during a certain time, Δt_{CL}, is lower than P_{thrs}.

3.4. Optimisation algorithm

The aim of the control strategy is to maximise the electricity production, i.e., the overall efficiency of the PTO. There are five unknown variables, a_{RO}, P_{thrs}, Δt_{CL}, Ω_{U}, Ω_{L}, which need to be evaluated to implement the control algorithm described in Section 3.3. A genetic algorithm [69] capable of converging to a global maximum while exploring different solutions is used to find the values for these variables.

In the current work, two optimisations are performed with the same genetic algorithm: optimisation of the (1) representative sea states and (2) extreme sea states.

The first optimisation aims to determine the value of the control parameter a_{RO} such that the total time-averaged efficiency, $\overline{\eta}_{\text{total}}$, is maximised for each representative sea state subset. The total time-averaged total efficiency is defined here as

$$\overline{\eta}_{\text{total}} = \overline{\eta}_{\text{turb}}\overline{\eta}_{\text{gen}}\,, \tag{14}$$

where

$$\overline{\eta}_{\text{turb}} = \frac{\overline{P}_{\text{turb}}}{\overline{P}_{\text{avail}}}, \tag{15}$$

and

$$\overline{\eta}_{\text{gen}} = \frac{\overline{P}_{\text{elec}}}{\overline{P}_{\text{turb}}}, \tag{16}$$

are, respectively, the turbine and generator time-averaged efficiencies. Here, the mean turbine power is,

$$\overline{P}_{\text{turb}} = \frac{1}{t_{\text{f}} - t_{\text{i}}}\int_{t_{\text{i}}}^{t_{\text{f}}} T_{\text{turb}}(t)\Omega(t)\text{d}t\,, \tag{17}$$

and the mean electrical power output is,

$$\overline{P}_{\text{elec}} = \frac{1}{t_{\text{f}} - t_{\text{i}}}\int_{t_{\text{i}}}^{t_{\text{f}}} \eta_{\text{gen}}\left(\Omega(t), \frac{P_{\text{gen}}(t)}{P_{\text{gen}}^{\text{rated}}}\right) P_{\text{gen}}(t)\,\text{d}t\,, \tag{18}$$

where η_{gen} is the efficiency of the generator (see Fig. 3), and $P_{\text{gen}}(t) = T_{\text{gen}}(t)\Omega(t)$ is the generator counter power.

The second optimisation aims to determine the variables P_{thrs}, Δt_{CL}, Ω_{U}, Ω_{L}, such that the mean annual electrical energy production, MAEP^{ext}, for the extreme sea state sub-set is maximised. The mean annual electrical energy production is given by

$$\text{MAEP}\,[\text{Wh}] = 8760\sum_{i=1}^{27}\overline{P}_{\text{elec}}^{\,i} f_{\text{o}}^{i}\,, \tag{19}$$

where $\overline{P}_{\text{elec}}^{\,i}$ and f_{o}^{i} are the average electrical power and frequency of occurrence of sea state i, respectively, see Fig. 5 b). The calculation of MAEP^{ext} is obtained from Eq. (19) considering the subset of extreme sea states.

The fitness function, constraints and optimisation problem for both optimisations are given in Table B.7 in Appendix B. The main features of the genetic algorithm and the stopping criteria for both optimisations are in Table B.8 in Appendix B. Both optimisation problems were solved using the *optimisation Tool* with the solver ga - *genetic algorithm* of MATLAB version 2020a.

3.5. Adjustment of variables and results comparison

The test results of the biradial turbine of the Mutriku wave power plant available in the Zenodo database cover two test periods. The first period corresponds to the operation of the frequency converter in a closed loop. These tests took place between July and December 2017. In the second period, the frequency converter controller operated the generator in an open loop. A $\text{d}V/\text{d}t$ filter was installed between the frequency converter and the biradial turbogenerator, separated by a distance of over 100 m. The second-period tests were conducted between January and June 2018. Increased electrical losses were observed in the second test arrangement, which affected the average electrical efficiency of the generator [48]. A fair comparison between the results of the present control algorithm and those developed and tested in the OPERA project is achieved by assuming the efficiency of the electric generator as measured in its dry tests at IST [47]. Their results are shown in Fig. 3. Therefore, a new post-processing of these test results was carried out, as described below:

1. Generator efficiency: The generator efficiency and electrical power are evaluated using the numerical model from the experimental characterisation [47] (see Fig. 3);

Table 3
Information about the tests used for the numerical validation.

Test number	H_s [m]	T_p [s]	$a \times 10^3$ [Nm s^b]	b [–]	rms(Ω) [rad/s]	rms(Δp) [kPa]
1	1.2	11.0	1.11	2.0	162	4.3
2	0.6	10.2	0.10	2.9	102	1.9
3	0.7	14.0	0.15	2.4	128	2.8
4	1.3	8.9	1.11	2.0	154	3.8

2. Counter torque of the generator: From the measured time series of the rotational speed and torque of the turbine shaft, the counter torque of the generator is calculated using Eq. (7);
3. When the high-speed safety valve or the plant's butterfly valve are closed, the available power and the turbine power are set to zero.

4. Analysis of the results

4.1. Pressure readings as input of the numerical model

As indicated in Section 3.2, the damping provided by the biradial turbine is weekly dependent on the rotational speed and has no significant influence on the hydrodynamic process of wave energy extraction by the WEC. Consequently, the time-domain numerical model can be simplified by neglecting the existence of the hydrodynamic conversion of energy from waves to pneumatic power, using the time series of the available pressure head of the turbine as input, regardless of the chosen turbine–generator control law. Comparing the numerical and experimental results implies that the same control algorithm must be applied for the same turbine pressure head. As described in Appendix A, the Zenodo's database does not provide the control algorithm parameters used for each test, which prevents the reproduction of the control algorithms. Instead, data collected by the IST team during the commissioning phase of the OPERA turbine–generator set at the Mutriku wave power plant is used here to validate the numerical model. From the collected data, information on the sea state conditions and the parameters of the control algorithm was recorded. Four CL1 tests of 30 min duration were selected for the proposed validation; see Table 1. The sea state conditions, control variables a and b, and root-mean-square of the rotational speed and turbine pressure head are shown in Table 3.

Fig. 7 shows the measured rotational speed (Experimental) together with the numerically determined values (Numerical) using the control law imposed at the test site. The data in Fig. 7 show considerable agreement between the experimental and numerical results of rotational speed with average and maximum errors of 3.5 rad/s and 7.5 rad/s, respectively. These errors are acceptable, considering the accuracy of the experimental data presented in Zenodo's database and the order of magnitude of the rotational speed. Therefore, the results evidence that the numerical model is suitable for carrying out the work programme proposed in this paper.

4.2. Optimisation for the representative cases

The control algorithm described in Section 3.3 was applied to the subset of 27 representative test cases in the Zenodo database. The optimisation results for the generator, turbine and time-averaged total efficiency are shown in Fig. 8 as a function of the root-mean-square of the turbine pressure head, rms(Δp). Note that the rms(Δp) value increases with the increasing energy of a given sea state. The rms(Δp) value ranges from 1.7 to 7.7 kPa for this subset of sea states.

Fig. 8 also shows boxplots of the generator load normalised by the rated power of the generator, P_{gen}/P_{gen}^{rated}, see Fig. 8 a), and the pressure coefficient normalised by the pressure coefficient at the best efficiency point, Ψ/Ψ_{bep}, see Fig. 8 b), for three cases corresponding to different values of rms(Δp), see Table 4. Furthermore, in Fig. 8 c), three regions can be seen where the variation of the time-averaged total efficiency $\overline{\eta}_{total}$ is significant. This variation corresponds to the different load characteristics imposed on the generator and the turbine. These regions are represented in Fig. 8 by white, grey and black symbols corresponding to different rms(Δp) ranges. Table 4 also shows the results of some helpful variables for analysing three cases within the identified rms(Δp) regions. Next, the behavioural analysis of the system for each identified region is presented.

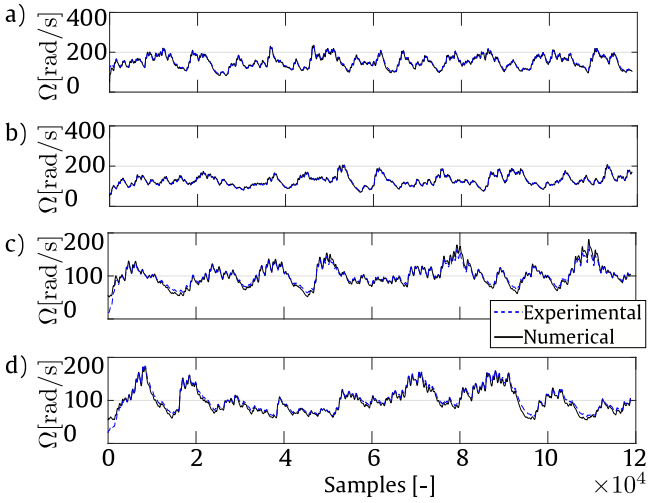

Fig. 7. Validation of the numerical model. Experimental (solid black lines) and numerical results (blue dashed lines): a) Test 1; b) Test 2; c) Test 3; and d) Test 4.

In region I, $\overline{\eta}_{total}$ increases with rms(Δp), mainly due to the increase in $\overline{\eta}_{gen}$. The increase in $\overline{\eta}_{gen}$ is due to the variation of generator's counter torque as a quadratic function of the rotational speed when it is operated at a generator power below the rated power ($T_{gen} = a_{RO}\Omega^2$), see Fig. 6. Thus, the turbine–generator set rotates faster when the available pneumatic power increases. Consequently, the power of the generator and its efficiency increase; see Fig. 3. As with standard squirrel-cage induction motors, the generator's efficiency reaches high values in the range of $\eta_{gen} = 0.70$ to 0.91 at low load (for this generator for $P_{gen}/P_{gen}^{rated} > 0.05$, see Fig. 3). In Fig. 8 a), the blue boxplot corresponding to Case 1 with a load rms(P_{gen})/P_{gen}^{rated} = 0.05 shows $\overline{\eta}_{gen} = 0.656$, well below the maximum value $\overline{\eta}_{gen} = 0.800$ observed at the end of the interval defining this region. A more detailed analysis of the optimisation results shows that a_{RO} is significantly larger than a_{bep} in region I, which is due to the high sensitivity of the electric generator efficiency to the generator counter torque at low energetic sea conditions, corresponding to a low rotational speed of the turbine–generator set, see Fig. 3. As shown by the blue boxplot in Fig. 8 a), the turbine is operated at higher values of pressure head coefficient Ψ than the value for the best average turbine efficiency to achieve a higher average electric generator efficiency, which more than compensates for the decrease in average turbine efficiency.

In region II, $\overline{\eta}_{total}$ increases slightly with the increase in rms(Δp). There is a tiny decrease in $\overline{\eta}_{turb}$ and a slight increase in $\overline{\eta}_{gen}$. The generator operates with higher loads than in Case 1, so its efficiency is higher. In Fig. 8 b) the green boxplot shows that the difference between the 25% and 75% percentiles of Ψ/Ψ_{bep} is smaller compared to Case 1, with the median value closer to 1, corresponding to a higher average turbine efficiency $\overline{\eta}_{turb}$. The small decrease in $\overline{\eta}_{turb}$ results from the higher accumulation of kinetic energy ($\frac{1}{2}I\Omega^2(t)$) in the rotational masses of the PTO when rms(Δp) and rms(Ω) increase.

In region III, $\overline{\eta}_{total}$ decreases with the increase in rms(Δp) due to the abrupt decrease in $\overline{\eta}_{turb}$. This decrease is due to the change of the control law from regular to safe-mode operation, which is required

Table 4
Three selected cases from the representative cases optimisation.

Case	$a_{RO} \times 10^3$ [Nm s^2]	$\overline{\eta}_{gen}$ [–]	$\overline{\eta}_{turb}$ [–]	$\overline{\eta}_{total}$ [–]	$\frac{rms(\Psi)}{\Psi_{bep}}$ [–]	min(Ω) [rad/s]	rms(Ω) [rad/s]	max(Ω) [rad/s]	$\frac{rms(P_{gen})}{P_{gen}^{rated}}$ [–]	rms(Δp) [kPa]	max(Δp) [kPa]
1 (blue)	2.89	0.656	0.565	0.370	2.73	41	75	115	0.05	1.7	5.8
2 (green)	2.86	0.809	0.574	0.464	2.56	50	147	277	0.39	6.0	24.7
3 (red)	2.86	0.809	0.536	0.433	3.75	50	144	301	0.53	7.7	34.3

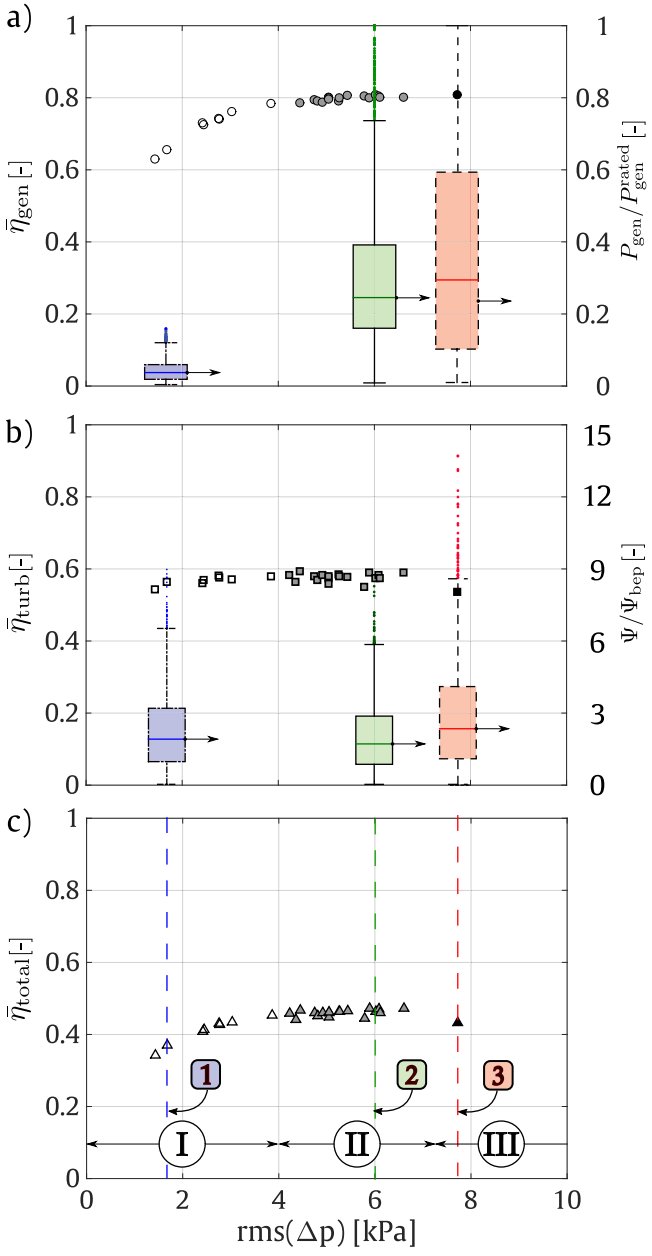

Fig. 8. Optimisation of representative cases: Generator, turbine and total time-averaged efficiencies, respectively, a), b) and c), as a function of the root-mean-square of the turbine pressure head, rms(Δp). Boxplots for the generator load normalised by the generator rated power, P_{gen}/P_{gen}^{rated}, and pressure coefficient normalised by the pressure coefficient at the best efficiency point, Ψ/Ψ_{bep}, for three cases: Case 1, blue, Case 2, green, Case 3, red, corresponding to different rms(Δp) values, see Table 4. Illustration of three regions with the variation of total time-averaged efficiency: Region I, II and III, corresponding to ranges of rms(Δp) : < 4.0 kPa, [4.0 kPa, 7.7 kPa], > 7.7 kPa.

to maintain the rated power and maximum rotational speed for long periods. In contrast to Case 2, the generator load in Case 3 shows greater variability and a higher occurrence of high loads (more occurrences of $P_{gen} = P_{gen}^{rated}$). These conditions are detrimental to the turbine performance and result in high Ψ peaks. At the same time, the generator's performance benefits from a high load (and thus high efficiency, see Fig. 3). Therefore, its $\overline{\eta}_{gen}$ does not change significantly compared to other cases studied. For rms(Δp) > 7.7 kPa, $\overline{\eta}_{total}$ is expected to decrease due to the high energy flux the PTO is subjected to, resulting in the turbine being operated in the safe mode for a longer time, further decreasing the turbine efficiency. Nevertheless, there is a limit of rms(Δp) above which the maximum rotational speed of the turbine–generator set is exceeded unless a relief valve connected in parallel with the turbine is open or a safety valve connected in series with the turbine is partially closed [38]. The control of such valves is beyond the scope of the present work, and their operation interferes with the hydrodynamic conversion of wave energy into pneumatic power, as mentioned in Section 3.2.

We use the air density, rotor diameter and root-mean-square of rotational speed, rms(Ω), to define the dimensionless control parameter, a^*, given by

$$a^* = \frac{a_{RO}}{\rho D^5 rms(\Omega)}. \tag{20}$$

Since the atmospheric conditions are not given in the Zenodo's data base, $\rho = 1.225\,kg/m^3$ is assumed.

A plot of a^* as a function of rms(Ω) is shown in Fig. 9, as is a^*_{bep} (corresponding to $a_{RO} = a_{bep}$, see Eq. (8)). At low rotational speeds, Fig. 9 shows a rapid decrease in a^* with increasing rms(Ω) in the region I, where the low generator load makes the generator efficiency most sensitive to the increase in generator load. At higher rotational speeds, a^* approaches the value corresponding to the highest turbine efficiency, a^*_{bep}, as the generator efficiency is nearly constant at the corresponding loads. The least-squares fitting of a^* versus rms(Ω) represented in Fig. 9 is given by

$$a^* \times 10^3 = \begin{cases} 1.524 & rms(\Omega) < 60\,rad/s \\ 391.2\,rms(\Omega)^{-1.355} & 60 \le rms(\Omega) < 166\,rad/s \\ 0.3838 & rms(\Omega) \ge 166\,rad/s \end{cases}, \tag{21}$$

with a coefficient of determination $R^2 = 0.95$. Since there is a clear correspondence between the fit and the data obtained from the optimisation, it is possible to perform real-time control where the parameter $a_{RO}(rms(\Omega))$ is updated at every given time interval. The sensitivity analysis results for different sea state conditions showed 6 s as a suitable time interval for updating the control parameter $a_{RO}(rms(\Omega))$.

4.3. Optimisation of extreme cases

When the 27 extreme cases were optimised, the genetic algorithm converged to $[P_{thrs}, \Omega_U, \Omega_L, \Delta t_{CL}] = [28\,kW, 155\,rad/s, 35\,rad/s, 12\,s]$. These results imply that if, during a time interval of 12 s, the mean available pneumatic power is greater than or equal to 28 kW and the rotational speed is greater than or equal to 155 rad/s, the safe mode is activated, which prescribes the maximum permissible torque for this PTO (see Fig. 6). Note that the converged value of Δt_{CL} is approximately in the middle of the range of peak times of the most common sea states, see Fig. 5 a).

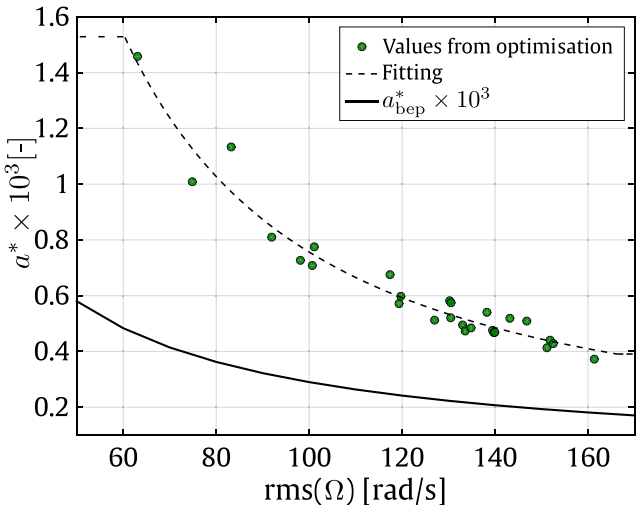

Fig. 9. Variation of a^* (green circles) and a^*_{bep} (solid black line) with the root-mean-square of rotational speed, rms(Ω). Fitting curve (dashed black line), see Eq. (21).

4.4. Comparison with Zenodo's database

The results from Sections 4.2 and 4.3 gave the best control law parameters for the construction of the proposed control algorithm. During regular operation (RO), the control law is defined as

$$T^{RO}_{gen} = \min\left(a_{RO}(\text{rms}(\Omega))\Omega^2,\ P^{rated}_{gen}/\Omega,\ T^{lim}_{gen}\right), \tag{22}$$

where $a_{RO}(\text{rms}(\Omega))$ is calculated from Eq. (21). Whenever the time-averaged available pneumatic power over $\Delta t_{CL} = 12$ s exceeds $P_{thrs} = 28$ kW and the rotational speed is higher than $\Omega_U = 155$ rad/s, the system enters into safe-mode (SM) operation. During SM operation, the control law is defined as

$$T^{SM}_{gen} = \min\left(P^{rated}_{gen}/\Omega,\ T^{lim}_{gen}\right). \tag{23}$$

Then the control algorithm returns to RO when the rotational speed is lower than $\Omega_L = 35$ rad/s. From now on, this control algorithm is called the Best Control Algorithm (BCA).

The BCA was used to control the PTO, and its results are compared below with all 257 test results available in the Zenodo database (see Section 3.5).

The results of the MAEP, the maximum rotational speed, the number of times the maximum rotational speed was exceeded and the number of times the high-speed safety valve was partially closed are shown for Zenodo's database and BCA in Table 5. MAEP is calculated using Eq. (19), taking into account all 257 test results available in the Zenodo database. For each of the 27 sea states represented in the database (see Fig. 5 c)), the mean time-averaged electrical power

$$\overline{P}^i_{elec} = (\sum_{j=1}^{N} \overline{P}^i_{elec\,j})/N \tag{24}$$

calculated from the N available test results j for each bin i, was taken into account in solving Eq. (19). Note also that the sum of all occurrence frequencies in Fig. 5 a) is 95.2% because there are bins in the Zenodo database without tests (see white bins in Fig. 5 a)). Here, the production corresponding to these empty bins is ignored. The results in Table 5 show that the BCA provides a noticeable increase in MAEP of 5.7% compared to the data in the Zenodo's database.

There are 27 tests where the maximum rotational speed was achieved. The following control law was applied to these cases to assess whether the designed control algorithm is robust enough (see Fig. 6):

$$T_{gen}(\Omega) = \min\left(P^{rated}_{gen}/\Omega,\ T^{lim}_{gen}\right). \tag{25}$$

Table 5
Comparison of the results of the Zenodo database and the BCA control. Without additional valve control, the BCA could not control 27 out of 257 test cases. Sixteen constantly apply the maximum permissible counter torque of the generator, marked *.

Case	MAEP [MWh]	max(Ω) [rad/s]	No. of tests with Ω_{max} exceeded	No. of tests with valve control
Zenodo's database	36.6	256	0	98
BCA	38.7	342 (420*)	11 (27*)	0

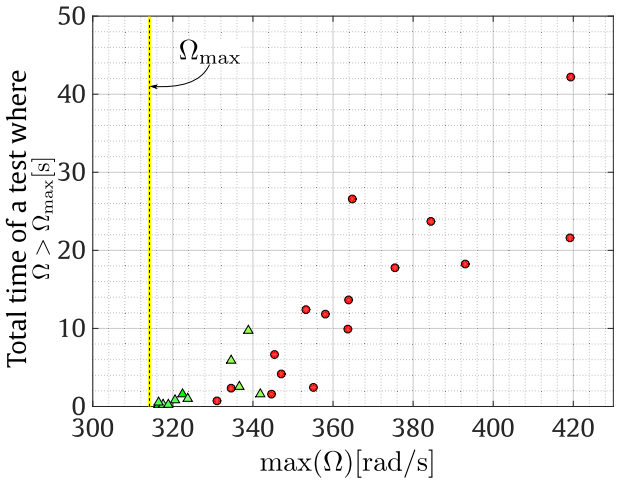

Fig. 10. Maximum rotational speed versus total time with rotational speed above maximum threshold Ω_{max} for tests requiring additional valve control. Green triangles — Eleven tests where the BCA could not control without valve control; Red circles — Sixteen tests where the maximum rotational speed was reached even though the maximum permissible counter torque of the generator was applied for the entire test duration.

Eq. (25) indicates the maximum permissible counter torque of the generator for any rotational speed that the generator can apply. The results show that the maximum rotational speed was reached in the 16 tests even when the maximum allowable counter torque of the generator was applied. From now on, these tests will be referred to as tests requiring additional valve control and will be analysed later in Section 4.5. In the remaining 11 cases, the maximum rotational speed with BCA control was 342 rad/s, Table 5. The control laws of the OPERA project required the actuation of the safety valve in 98 of 257 test cases, while the BCA could not control only 27 test cases without additional valve control.

Fig. 10 shows the maximum rotational speed for a given test and the total time during which the rotational speed was higher than the maximum rotational speed. Although the BCA presents 11 tests where the maximum rotational speed was exceeded in approximately 8% of the maximum design rotational speed, the effects during one year of operation do not threaten the integrity of the PTO due to the low frequency of occurrence. Analysis of these 11 tests in the Zenodo's database shows that the high-speed safety valve was used to limit the rotational speed by immediately shutting off the flow rate into the turbine, and thus the pneumatic power, as soon as the maximum allowable rotational speed was reached.

It is important to reiterate that in the Zenodo's database tests, it was possible to use the high-speed safety valve on the turbine to protect the PTO. This is not the case with the BCA control algorithm discussed in this paper. An additional valve control loop is required for the turbine–generator set to operate across all 257 test cases in the Zenodo database.

Fig. 11 shows the time-averaged generator, turbine and total efficiencies as a function of root-mean-square of turbine pressure head.

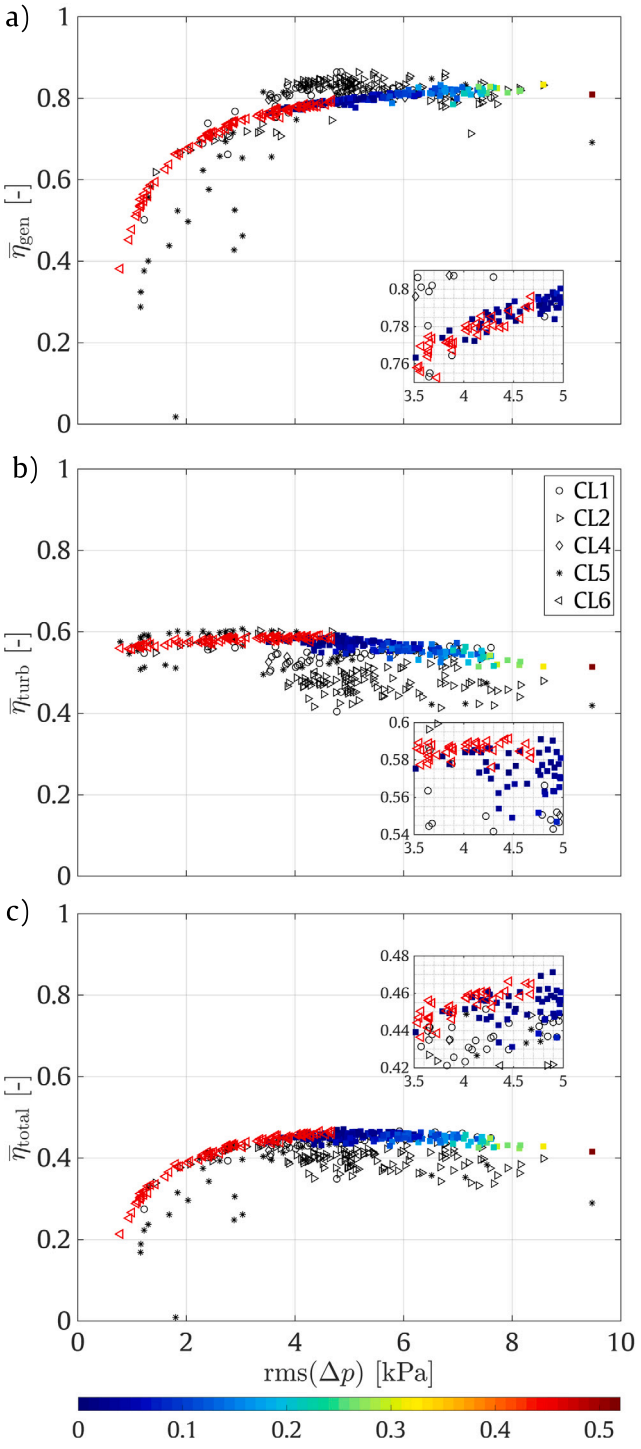

Fig. 11. Time-averaged total, turbine and generator efficiencies as a function of the root-mean-square of turbine pressure head. Zenodo's database results (see Table 1): Black markers; BCA results: Regular operation — red triangles; Safe-mode on — circles filled with a jet colour palette representing the percentage of time in safe-mode, varying from 0 to 52%.

Black open symbols refer to the Zenodo database results. Open red triangles show the BCA results at the regular operation during the test period. In contrast, squares filled with the jet colour palette represent the test results when operating in safe mode between 0 and 52% of the time (maximum percentage of time tested in the calculations).

A clear difference in the scatter between Zenodo's database, and BCA results can be seen in Fig. 11. This result was expected since the goal of the experimental campaign that produced the Zenodo database results, as opposed to the structured control algorithm of the present work, was to test different control algorithms to see which would perform better.

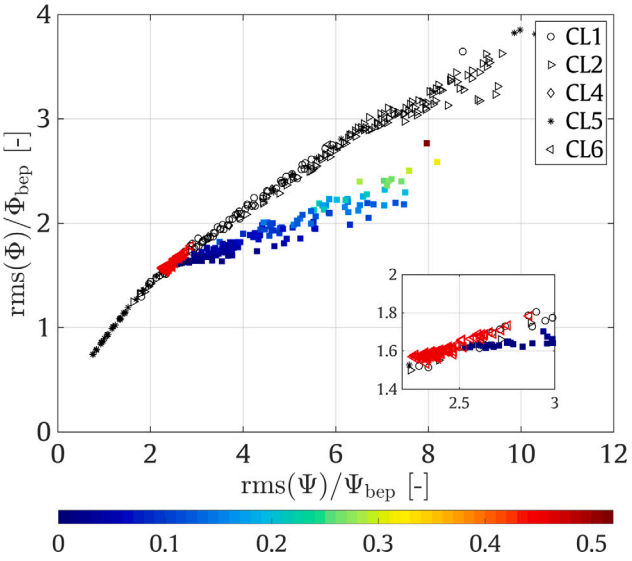

Fig. 12. Normalised root-mean-square of flow coefficient versus normalised root-mean-square of the dimensionless pressure head. Zenodo's database results (see Table 1): Black symbols; BCA results: Regular operation — red triangles; Safe-mode on — circles filled with a jet colour palette representing the percentage of time in safe-mode, varying from 0 to 52%.

The results show that the control algorithms in the Zenodo's database perform better in ensuring higher time-averaged efficiency of the generator, see Fig. 11 a). The time-averaged efficiency of the generator is higher for a large part of the tests for Zenodo's database than for BCA. For rms(Δp) > 4 kPa, the value is above 0.80 (except for rms(Δp) > 9 kPa; this particular test result will be analysed later) and appears to plateau around this value. In contrast, BCA shows a monotonic increase in this variable up to rms(Δp) > 9 kPa. The same cannot be said regarding the time-averaged efficiency of the turbine, where BCA remarkably out-stood for a great part of the tests, see Fig. 11 b). Since the ultimate goal is to maximise the time-averaged overall efficiency, BCA shows significantly better results overall, see Fig. 11 c). This confirms the increase in MAEP shown in Table 5.

With BCA, the safe mode is turned on when needed. Fig. 11 shows that for rms(Δp) < 3.5 kPa safe mode was not used due to the relatively low relation between pneumatic and generator power. In this range, the $\overline{\eta}_{turb}$ increased with increasing rms(Δp) because the efficiency of the electric generator decreases at higher loads (this result was previously justified, see Section 4.2). In these cases, the turbine operates under near-optimal conditions (see Fig. 6), most of the time with the control law $T_{gen}^{RO}(\Omega(t)) = a_{RO}(\text{rms}(\Omega(t)))\Omega^2(t)$, and only a few times in $T_{gen}^{SM}(\Omega(t)) = \min\left(P_{gen}^{rated}/\Omega(t), T_{gen}^{lim}\right)$. These conditions greatly benefit the efficiency of the turbine. This is confirmed by the position of the open symbols in Fig. 12, where the operating range of Ψ (or Φ) is narrow and close to Ψ_{bep} (or Φ_{bep}). If the inertia of the PTO was virtually zero, one could keep $\Psi = \Psi_{bep}$. Since a real PTO has inertia and the pressure head of the turbine (and thus the flow rate) is not constant in time, to maximise $\overline{\eta}_{turb}$, one must control the biradial turbine so that $\Psi > \Psi_{bep}$ to operate the turbine at a high efficiency most of the time. As can be seen in Fig. 12, the Ψ/Ψ_{bep} in normal operation is between 2 and 5 (see Fig. 2). For rms(Δp) > 3.5 kPa, the safe mode was on, prescribing the maximum torque in some periods and reducing $\overline{\eta}_{turb}$. To illustrate this statement, assume that for a certain time t the rotational speed is $\Omega(t)$ and two situations both operating in RO and $T_{gen}^{RO}(\Omega(t)) = a_{RO}(\text{rms}(\Omega(t)))\Omega^2(t)$. At the next time-step, $t + 1$,

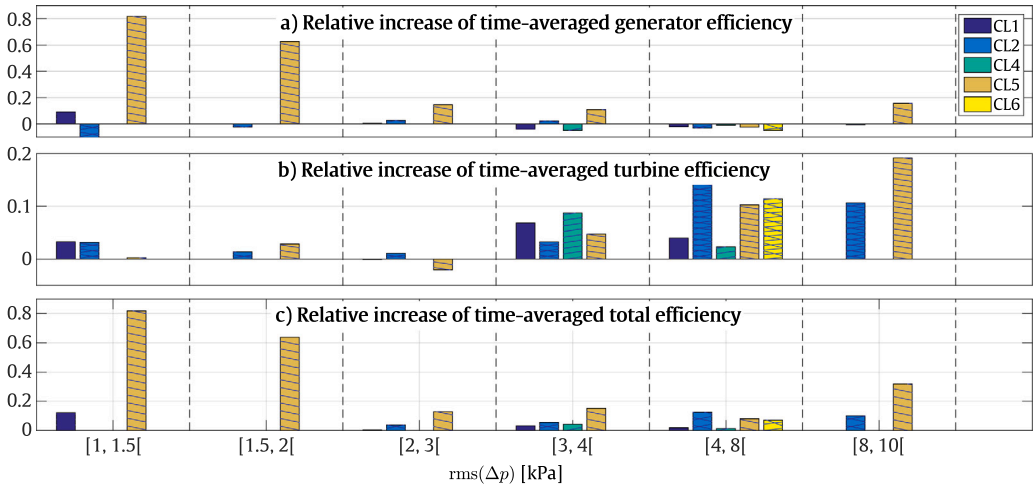

Fig. 13. Mean relative increase in time-averaged total, turbine and generator efficiencies by the present BCA control algorithm compared to the control laws of the project OPERA (see Table 1) for representative ranges of the root-mean-square of turbine pressure head.

there is a need to operate in the safe mode in the second situation. Assume that the turbine pressure head is similar in both situations, so that $\Delta p^{\mathrm{RO}}(t+1) = \Delta p^{\mathrm{SM}}(t+1) = \Delta p(t+1)$. If safe mode operation is on, then $T_{\mathrm{gen}}^{\mathrm{SM}}(t+1) > T_{\mathrm{gen}}^{\mathrm{RO}}(t+1)$ and consequently $\Omega^{\mathrm{SM}}(t+1) < \Omega^{\mathrm{RO}}(t+1)$. Therefore, it follows from Eq. (1), $\Psi^{\mathrm{SM}}(t+1)$ is necessarily higher than $\Psi^{\mathrm{RO}}(t+1)$: $\Psi^{\mathrm{SM}}(t+1) = \Psi^{\mathrm{RO}}(t+1)\left(\Omega^{\mathrm{RO}}(t+1)/\Omega^{\mathrm{SM}}(t+1)\right)^2$. The efficiency of the turbine will inevitably decrease if more instances of $\Psi \gg \Psi_{\mathrm{bep}}$ appear during a particular test. So more time in safe mode means lower turbine efficiency and a high frequency of occurrence of $\Psi \gg \Psi_{\mathrm{bep}}$. In contrast, when entering safe mode, the $\overline{\eta}_{\mathrm{gen}}$ benefits from its high efficiency both in terms of rated power ($T_{\mathrm{gen}}(t) = P_{\mathrm{gen}}^{\mathrm{rated}}/\Omega$) and maximum generator counter torque ($T_{\mathrm{gen}}^{\mathrm{lim}}$), see Fig. 3.

Fig. 13 highlights the differences between the performance results shown in Fig. 11 for each OPERA's control algorithm [51] and the present control algorithm. The bar graphs in Fig. 13 represent the mean relative increase in time-averaged generator, turbine and overall efficiencies achieved by the present control algorithm compared to each of the OPERA control laws (see Table 1) in representative ranges of the root-mean-square of turbine pressure head rms(Δp). If the bar is above (below) zero, it means that the BCA control algorithm provides higher (lower) time-average efficiency than the control algorithms of Ref. [51]. The first important observation is the lack of test results in some ranges of root-mean-square of the turbine pressure head. Indeed, the analysis of the Zenodo database shows that not all the proposed control algorithms have been tested under similar sea state conditions (see, for example, the absence of some bars, namely for CL6, which is only present within the range $8\,\mathrm{kPa} > \mathrm{rms}(\Delta p) \geq 4\,\mathrm{kPa}$). The control law CL5 is the one that shows results in each of the investigated ranges. Except for CL5, the control laws of the OPERA project favour the average efficiency of the electric generator Fig. 13 a) but disfavour excessively the average efficiency of the turbine Fig. 13 b) compared to the present BCA control law. As a result, the BCA control algorithm outperforms all OPERA's control laws, especially for $\mathrm{rms}(\Delta p) > 2\,\mathrm{kPa}$, as shown in Fig. 13 c).

A feature of the PTO control algorithm is the ratio between the maximum and root-mean-square of the generator's counter torque,

$$\tau = \frac{\max(T_{\mathrm{gen}})}{\mathrm{rms}(T_{\mathrm{gen}})}. \tag{26}$$

Ideally, τ should not be too large. Otherwise, generator fatigue can lead to reliability problems (e.g., damage to the generator windings) if it is not already considered in the specification of the electric generator. For an OWC PTO like this, where the rotating masses have a relatively low moment of inertia and $\max(\Delta p)/\mathrm{rms}(\Delta p) \gg 1$, it is not possible to have $\tau \approx 1$. Fig. 14 a) shows τ as a function of root-mean-square of turbine pressure head for tests where only RO was used (black triangles) and where SM operation was enabled (blue squares). The

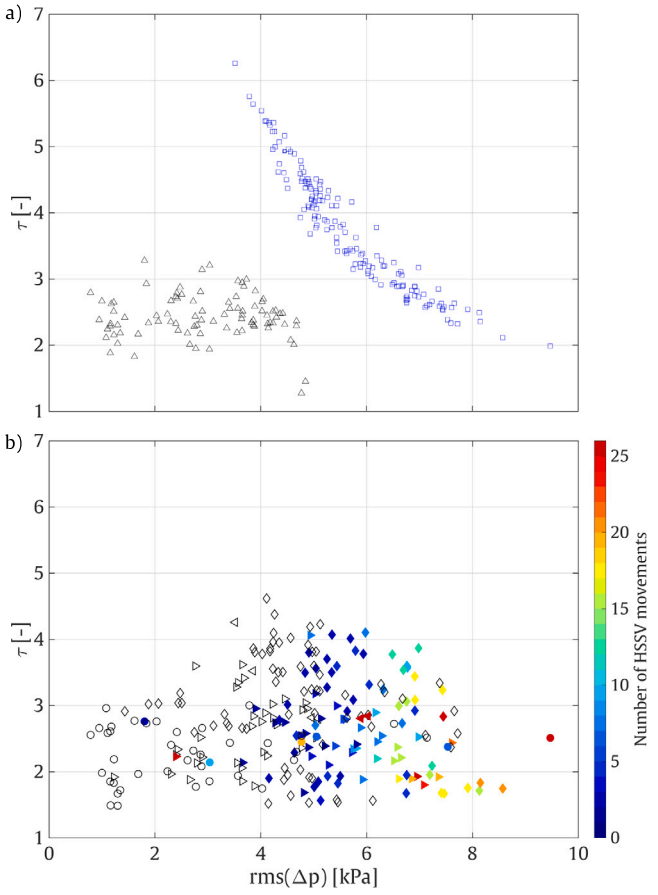

Fig. 14. Ratio between the maximum and the root-mean-square counter torque of the generator, τ, as a function of the root-mean-square of the turbine pressure head. (a) BCA control algorithm with the regular operation (black triangles) and safe-mode operation activated when required (blue squares), without safety valve operation. (b) Tests of OPERA control laws without the use (open symbols) and with the use (solid symbols) of the high-speed safety valve; CL1 — right triangles; CL2 — diamonds; CL4 — left triangles; CL5 — circles; the symbols are filled with a jet colour palette representing times the high-speed safety valve is actuated in 15 min intervals.

inspection of Fig. 14 a) shows similar values between the tests in RO and when SM was activated in the ranges of turbine pressure heads of rms(Δp) < 3.5 kPa and 6 kPa < rms(Δp) < 10 kPa. In the tests performed only in RO, the imposed control algorithm had no τ discontinuities, and the counter torque of the generator followed $T_{gen}^{RO} = \min\left(a_{RO}(\text{rms}(\Omega(t)))\Omega^2(t), P_{gen}^{rated}/\Omega(t)\right)$. The same is true for the tests that operated in SM in the range 6 kPa < rms(Δp) < 10 kPa, as it was found that the control algorithm entered SM when the control law was $T_{gen}^{SM}(t) = P_{gen}^{rated}/\Omega(t)$.

From the results in Fig. 14 a) it is also evident that in the range of turbine's pressure heads 3.5 kPa < rms(Δp) < 6.0 kPa there was a significant difference between the tests where only RO and with SM was activated. Depending on whether or not the rotational speed before entering SM was closer to $\Omega = (P_{gen}^{rated}/a_{RO})^{1/3}$, the difference in the counter torque of the generator could be lower or higher. The evaluation of these variables during one year of operation gives an average value of $\tau = 2.7$, which seems to be a relatively favourable value concerning the fatigue of the electric generator components.

The comparison of Fig. 14 (a) and 14 (b) shows a larger scatter of the parameter τ for the control laws of the project OPERA compared to the BCA control law, which does not exceed $\tau = 5$. This is achieved by the intensive operation of the high-speed safety valve for rms(Δp) > 4 kPa, which may raise reliability concerns.

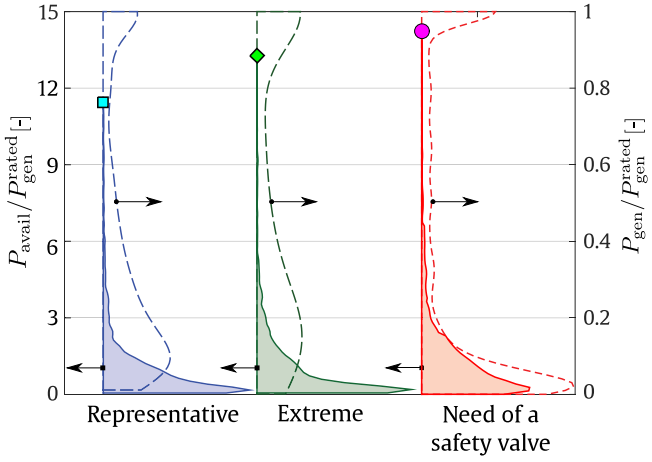

Fig. 15. Half-violin plots from representative (blue line), extreme (green line) and cases requiring safety valve operation (red line) for $P_{avail}/P_{gen}^{rated}$ (dashed line) and P_{gen}/P_{gen}^{rated} (solid line). The square, diamond and circle symbols present the maximum value of $P_{avail}/P_{gen}^{rated}$ for each case.

4.5. Cases requiring safety valve operation

The Zenodo's database show that the BCA control algorithm did not prevent the turbine from exceeding the maximum speed in 16 out of 257 tests. Not even this situation was avoided when the maximum counter torque of the generator was constantly applied, see Section 4.4. Fig. 15 shows half-violin plots of the pneumatic and generator power normalised to the generator's rated power, $P_{avail}/P_{gen}^{rated}$ and P_{gen}/P_{gen}^{rated}, for three different cases: representative, extreme and need of safety valve.

Observation of the half-violins plots in Fig. 15 corresponding to $P_{avail}/P_{gen}^{rated}$ (filled ones) indicates a very high frequency of occurrence for $P_{avail}/P_{gen}^{rated} < 2$ for any case. This result shows that the generator's rated power fits the available pneumatic power met at Mutriku's wave power plant. However, comparing the cases for each operating range of $P_{avail}/P_{gen}^{rated}$, it can see that the case labelled 'Need of a safety valve' occurs more frequently at higher values of $P_{avail}/P_{gen}^{rated}$ and also has the highest value of $P_{avail}/P_{gen}^{rated}$ (close to 15). Plotting turbine pressure head, pneumatic power, rotational speed and generator power as a function of time for the three cases in Fig. 16 shows that a group of waves may induce very high turbine pressure head peaks in short periods.

From the point of view of PTO control, the problem is not the occasional occurrence of high-pressure peaks and as a consequence of the available pneumatic power (see the range 400 s > t > 350 s in Fig. 16), nor a high occurrence of $P_{avail}/P_{gen}^{rated} < 2$, as observed in Fig. 15. The problem is the duration of the wave group with high-pressure peaks resulting in a strong acceleration of the PTO. Such excessive available pneumatic power significantly hinders the control of the PTO. Moreover, in cases like the one presented here, where the rms(Δp) is relatively low, it is even more difficult, as it was not foreseen that this case would be problematic.

Although these tests occur very rarely, common sense dictates that the design of a control algorithm should not allow for these situations. A safety control valve (slow or high-speed) must be installed in series or parallel with a PTO component. The control algorithm strategy is the same as the one described and analysed in this paper, in addition to a master control unit that checks if the accumulated energy is above a certain safety threshold that triggers the valve operation. As mentioned

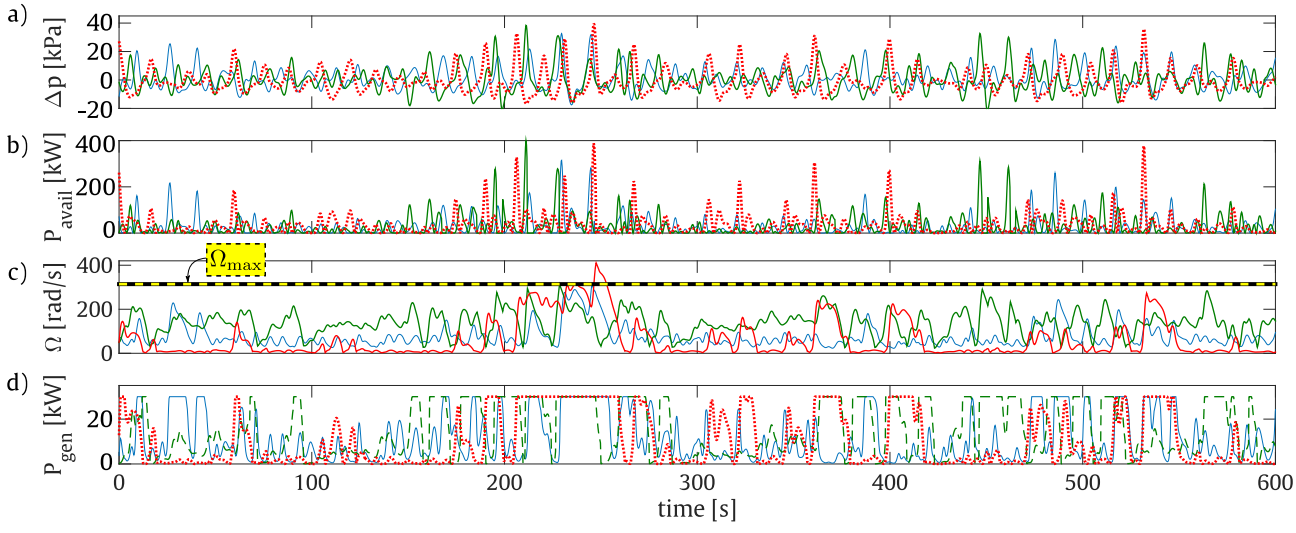

Fig. 16. Pressure head, rotational speed and counter torque of the generator as a function of time for three cases: Case 1, representative (green dotted line), Case 2, extreme but controllable (solid red line) and Case 3, extreme, requiring the operation of the safety valve (blue dash-dotted line).

earlier, the numerical model does not model the hydrodynamics of the OWC chamber. Therefore, the actuation of the safety valve was not investigated due to its influence on the hydrodynamics of the system.

4.6. Implementation of the control algorithm into real applications

The implementation of the novel control law under real conditions requires the use of hardware and software.

The hardware is an encoder, pressure, humidity and temperature sensors to measure the rotational speed and calculate the available pneumatic power. The PLC reads the above variables and controls the turbine–generator set by providing the torque control setpoint to the control unit of the variable frequency drive. The variable frequency drive must operate in close-loop torque-control mode with encoder.

Master–slave software must be implemented in the PLC. The master monitors the rotational speed, and a low-speed safety valve is actuated when the maximum threshold rotational speed is reached. The slave software follows the control strategy described in the paper.

5. Conclusions

A novel control algorithm for a turbine–generator set to equip oscillating-water-column devices was designed according to a detailed method to maximise energy production while ensuring the safe and reliable operation of the system. The algorithm has a master–slave control strategy. During regular operation, the algorithm follows a control law that increases the counter torque of the generator quadratically with speed and maximises the overall efficiency of the turbine–generator set on a time average. The algorithm checks the time-averaged available pneumatic power of the turbine over a backward time horizon. If the time-averaged pneumatic power and rotational speed are above certain thresholds, the safe-mode operation is switched on, and the generator's maximum permissible counter torque is set. The algorithm can be easily integrated into an industrial programmable logic controller that uses as inputs the rotational speed and turbine pressure head from an encoder assembled into the turbine shaft and pressure sensors on the pneumatic chamber, respectively. A genetic algorithm optimised the variables required to achieve the set goal.

A numerical model with input field data from the Mutriku wave power plant is used to simulate the performance of OPERA's biradial turbine–generator set. Comparing the results of the control algorithms of the project OPERA with those of the novel BCA control algorithm for the 257 test results available in Zenodo's public database, it is concluded that:

- The BCA control algorithm achieves a significant 6% increase in average annual electricity generation compared to OPERA's control laws.
- In general, OPERA's control laws favour the average efficiency of the electric generator but disfavour the average efficiency of the turbine excessively compared to the BCA control law.
- OPERA's control laws required the high-speed safety valve to operate in 98 of 257 test cases, while the BCA could not control only 11 test cases without additional valve control.
- The BCA control algorithm results in higher ratios between the maximum and root-mean-square of the generator's counter torque, which must be considered in the electric generator specification to avoid reliability problems due to generator winding fatigue.
- The OPERA's control laws require the intensive operation of the high-speed safety valve for $\mathrm{rms}(\Delta p) > 4\,\mathrm{kPa}$, which can lead to reliability concerns.
- Unlike some existing control algorithms, prediction of sea state conditions is not required, avoiding relying on online wave measurement systems near the OWC device, whose reliability is questionable.

Some tests have shown that the control algorithm did not prevent turbine overspeed. These tests present wave groups producing high time-averaged pressure peaks of excessive duration for the generator's rated power.

Although it is possible to predict the resource reaching a particular wave energy converter a few days in advance, unexpected wave groups can reach the system and cause undesirable energy peaks. Common sense engineering rules dictate that a safety valve (not modelled in this paper) is triggered whenever the accumulated energy is above a certain threshold. Note that this control law does not need to predict the coming wave. It uses the accumulated energy to determine whether the operation is safe.

The novel BCA control algorithm was developed for a biradial turbine. However, it is also expected to apply to axial impulse air turbines.

CRediT authorship contribution statement

A.A.D. Carrelhas: Conceptualization, Methodology, Software, Investigation, Formal analysis, Data curation, Visualization, Writing – original draft. **L.M.C. Gato:** Conceptualization, Methodology, Supervision, Formal analysis, Validation, Writing – original draft, Resources, Project administration, Funding acquisition.

Declaration of competing interest

The authors declare that they have no known competing financial interests or personal relationships that could have appeared to influence the work reported in this paper.

Data availability

Data will be made available on request.

Acknowledgements

This research was partially supported by European Union's Horizon 2020 Research and Innovation Programme under Grant Agreement No. 654444 (OPERA Project) and the Portuguese Foundation for Science and Technology - FCT, through IDMEC, under LAETA, project UIDB/50022/2020, and project MIT-EXPL/SOE/0094/2019. We acknowledge OPERA's partners Ente Vasco de la Energia, IDOM, Tecnalia, and Kymaner for their support during sea trials.

Appendix A. Zenodo's database

The collected data can be downloaded from the Zenodo repository [59]. There are 257 tests in HDF5 files with the following designation: OPERA_PP_YYYYMMDD_HHhMMmSS.h5, where YYYY is the year, MM is the month, DD is the day, HH, MM and SS are the hour, minute and second of the start of the test, respectively. Each file has two groups: "Values" and "TimeSeries". In the "Values" group, it is the control law type used, and some mean and root-mean-square values of power, control variables, and turbine coefficients, see Table A.6. In the "TimeSeries" group, it is the time series of essential variables to characterise the turbine's performance fully; see Table A.6.

In this database, some variables are missing that are needed to perform a numerical study like the one presented in this paper: (1) the air density in the turbine gallery and the pneumatic chamber; (2) the sea state conditions, i.e. the significant wave height and the peak (or energy) period; and (3) the parameters of the control law, e.g. for the case of CL1 the control parameters a and b are not mentioned. Therefore, it is not possible to accurately replicate the above tests.

Table A.6
List of variables in each group of the HDF5 files [57].

Values	TimeSeries
Dataset 'CL'	
Dataset 'Eta_Mean'	Dataset 'Delta_p'
Dataset 'Omega_Mean'	Dataset 'Eta'
Dataset 'Pdrive_Mean'	Dataset 'HSSV'
Dataset 'Pgrid_Mean'	Dataset 'Omega'
Dataset 'Pi_Mean'	Dataset 'Pdrive'
Dataset 'Ppneu_Mean'	Dataset 'Pgrid'
Dataset 'Pturb_Mean'	Dataset 'Phi'
Dataset 'RMS_Omega'	Dataset 'Pi'
Dataset 'RMS_Phi'	Dataset 'Ppneu'
Dataset 'RMS_Pi'	Dataset 'Psi'
Dataset 'RMS_Psi'	Dataset 'Pturb'
Dataset 'RMS_Q'	Dataset 'Q'
Dataset 'RMS_p'	Dataset 'damper'
Dataset 'TimeStamp'	Dataset 'time'

Table B.7
Genetic algorithm: Fitness function, constraints and optimisation problem for optimisation of representative (1) and extreme (2) cases.

Case	Fitness function	Constraints	Optimisation problem	
1	$\bar{\eta}_{\text{total}} = \bar{\eta}_{\text{turb}}\bar{\eta}_{\text{gen}}$	$10^{-6} < a_{\text{RO}} < 10^{2}$ $\Omega(t) < \Omega_{\max}$	minimise subject to $10^{-6} < a_{\text{RO}} < 10^{2}$ $\Omega(t) < \Omega_{\max}$	$F_1 = 1 - \bar{\eta}_{\text{total}}$
2	MAEP^{ext}	$P_{\text{gen}}^{\text{rated}} \le P_{\text{thrs}} \le 3P_{\text{gen}}^{\text{rated}}$ $\Omega_{\text{rated}} \le \Omega_{\text{U}} \le \Omega_{\text{rated}}$ $\frac{P_{\text{gen}}^{\text{rated}}}{T_{\text{gen}}^{\text{lim}}} \le \Omega_{\text{L}} \le \frac{1}{2}\Omega_{\max}$ $\Omega_{\text{U}} > \Omega_{\text{L}}$ $\Omega(t) < \Omega_{\max}$	minimise subject to $P_{\text{gen}}^{\text{rated}} \le P_{\text{thrs}} \le 3P_{\text{gen}}^{\text{rated}}$ $\Omega_{\text{rated}} \le \Omega_{\text{U}} \le \Omega_{\text{rated}}$ $\frac{P_{\text{gen}}^{\text{rated}}}{T_{\text{gen}}^{\text{lim}}} \le \Omega_{\text{L}} \le \frac{1}{2}\Omega_{\max}$ $\Omega_{\text{U}} > \Omega_{\text{L}}$ $\Omega(t) < \Omega_{\max}$	$F_2 = 1 - \frac{\text{MAEP}^{\text{ext}}}{\text{MAEP}^{\text{ref}}}$

Table B.8
Genetic algorithm: Main characteristics and stopping criteria for both optimisations.

Optimisation	1, Representative	2, Extreme
Reproduction - Main characteristics		
Size	400	1500
Fitness scaling	Rank	
Selection	Roulette-wheel	
Mutation	Adaptive feasible	
Crossover	0.8	
Elite	Elite	
Stopping criteria		
Maximum number of generations	25	100
Fitness limit	0.37	1
Stall limit	5	
Tolerance function	10^{-5}	

Appendix B. Genetic algorithm

Table B.7 lists the fitness function, F_i, the constraints and the optimisation problem for both optimisations. For the extreme sub-set optimisation, the objective function was set to a minimisation problem where MAEP^{ref} is a reference value that ensures that $0 \le F_2 \le 1$. Table B.8 shows the main features and stopping criteria for both optimisations.

References

[1] IPCC. Climate change 2021: The physical science basis. Contribution of working group I to the sixth assessment report of the intergovernmental panel on climate change. Cambridge, United Kingdom and New York, NY, USA: Cambridge University Press; 2021.

[2] Lenton T, Rockström J, Gaffney O, Rahmstorf S, Richardson K, Steffen W, et al. Climate tipping points - too risky to bet against. Nature 2019;575:592–5. http://dx.doi.org/10.1038/d41586-019-03595-0.

[3] D'Adamo I, Rosa P. Current state of renewable energies performances in the European Union: A new reference framework. Energy Convers Manage 2016;121:84–92. http://dx.doi.org/10.1016/j.enconman.2016.05.027.

[4] He Y, Liu Y, Du M, Zhang J, Pang Y. Comprehensive optimisation of China's energy prices, taxes and subsidy policies based on the dynamic computable general equilibrium model. Energy Convers Manage 2015;98:518–32. http://dx.doi.org/10.1016/j.enconman.2015.03.010.

[5] Tsao Y-C, Vu T-L, Lu J-C. Pricing, capacity and financing policies for investment of renewable energy generations. Appl Energy 2021;303:117664. http://dx.doi.org/10.1016/j.apenergy.2021.117664.

[6] Augutis J, Martisauskas L, Krikctolaitis R. Energy mix optimization from an energy security perspective. Energy Convers Manage 2015;90:300–14. http://dx.doi.org/10.1016/j.enconman.2014.11.033.

[7] Zappa W, Junginger M, van den Broek M. Is a 100% renewable European power system feasible by 2050? Appl Energy 2019;233–234:1027–50. http://dx.doi.org/10.1016/j.apenergy.2018.08.109.

[8] Weiss CVC, Guanche R, Ondiviela B, Castellanos OF, Juanes J. Marine renewable energy potential: A global perspective for offshore wind and wave exploitation. Energy Convers Manage 2018;177:43–54. http://dx.doi.org/10.1016/j.enconman.2018.09.059.

[9] Hoseinpoori P, Olympios AV, Markides CN, Woods J, Shah N. A whole-system approach for quantifying the value of smart electrification for decarbonising heating in buildings. Energy Convers Manage 2022;268:115952. http://dx.doi.org/10.1016/j.enconman.2022.115952.

[10] Jin X, Liu B, Liao S, Cheng C, Li G, Liu L. Impacts of different wind and solar power penetrations on cascade hydroplants operation. Renew Energy 2022;182:227–44. http://dx.doi.org/10.1016/j.renene.2021.10.022.

[11] Carballo R, Iglesias G. A methodology to determine the power performance of wave energy converters at a particular coastal location. Energy Convers Manage 2012;61:8–18. http://dx.doi.org/10.1016/j.enconman.2012.03.008.

[12] López I, Carballo R, Iglesias G. Site-specific wave energy conversion performance of an oscillating water column device. Energy Convers Manage 2019;195:457–65. http://dx.doi.org/10.1016/j.enconman.2019.05.030.

[13] Izquierdo M, Carrillo M. Optimization of aquaculture systems in Spain. Energy Convers Manage 1997;38(9):879–88. http://dx.doi.org/10.1016/S0196-8904(96)00094-5.

[14] Fox BN, Gomes RPF, Gato LMC. Analysis of oscillating-water-column wave energy converter configurations for integration into caisson breakwaters. Appl Energy 2021;295:117023. http://dx.doi.org/10.1016/j.apenergy.2021.117023.

[15] Henriques JCC, Portillo JCC, Gato LMC, Gomes RPF, Ferreira DN, Falcão AFO. Design of oscillating-water-column wave energy converters with an application to self-powered sensor buoys. Energy 2016;112:852–67. http://dx.doi.org/10.1016/j.energy.2016.06.054.

[16] Oikonomou CLG, Gomes RPF, Gato LMC. Unveiling the potential of using a spar-buoy oscillating-water-column wave energy converter for low-power stand-alone applications. Appl Energy 2021;292:116835. http://dx.doi.org/10.1016/j.apenergy.2021.116835.

[17] Robertson B, Bekker J, Buckham B. Renewable integration for remote communities: Comparative allowable cost analyses for hydro, solar and wave energy. Appl Energy 2020;264:114677. http://dx.doi.org/10.1016/j.apenergy.2020.114677.

[18] IRENA. Fostering a blue economy: Offshore renewable energy. Abu Dhabi: International Renewable Energy Agency; 2020, URL https://www.irena.org/-/media/Files/IRENA/Agency/Publication/2020/Dec/IRENA_Fostering_Blue_Economy_2020.pdf.

[19] Cazzaro D, Trivella A, Corman F, Pisinger D. Multi-scale optimization of the design of offshore wind farms. Appl Energy 2022;314:118830. http://dx.doi.org/10.1016/j.apenergy.2022.118830.

[20] Bertram D, Tarighaleslami A, Walmsley M, Atkins M, Glasgow G. A systematic approach for selecting suitable wave energy converters for potential wave energy farm sites. Renew Sustain Energy Rev 2020;132:110011. http://dx.doi.org/10.1016/j.rser.2020.110011.

[21] Tay ZY. Energy generation enhancement of arrays of point absorber wave energy converters via Moonpool's resonance effect. Renew Energy 2022;188:830–48. http://dx.doi.org/10.1016/j.renene.2022.02.060.

[22] Gomes RPF, Gato LMC, Henriques JCC, Portillo JCC, Howey BD, Collins KM, et al. Compact floating wave energy converters arrays: Mooring loads and survivability through scale physical modelling. Appl Energy 2020;280:115982. http://dx.doi.org/10.1016/j.apenergy.2020.115982.

[23] Portillo JCC, Collins KM, Gomes RPF, Henriques JCC, Gato LMC, Howey BD, et al. Wave energy converter physical model design and testing: The case of floating oscillating-water-columns. Appl Energy 2020;278:115638. http://dx.doi.org/10.1016/j.apenergy.2020.115638.

[24] López I, Carballo R, Iglesias G. Intra-annual variability in the performance of an oscillating water column wave energy converter. Energy Convers Manage 2020;207:112536. http://dx.doi.org/10.1016/j.enconman.2020.112536.

[25] Zheng X, Ji M, Jing F, Lu Y, Zheng W, Zhou S, et al. Sea trial test on offshore integration of an oscillating buoy wave energy device and floating breakwater. Energy Convers Manage 2022;256:115375. http://dx.doi.org/10.1016/j.enconman.2022.115375.
[26] Arena F, Laface V, Malara G, Romolo A, Viviano A, Fiamma V, et al. Wave climate analysis for the design of wave energy harvesters in the Mediterranean Sea. Renew Energy 2015;77:125–41. http://dx.doi.org/10.1016/j.renene.2014.12.002.
[27] Portillo JCC, Reis PF, Henriques JCC, Gato LMC, Falcão A. Backward bent-duct buoy or frontward bent-duct buoy? Review, assessment and optimisation. Renew Sustain Energy Rev 2019;112:353–68. http://dx.doi.org/10.1016/j.rser.2019.05.026.
[28] Setoguchi T, Takao M. Current status of self rectifying air turbines for wave energy conversion. Energy Convers Manage 2006;47(15):2382–96. http://dx.doi.org/10.1016/j.enconman.2005.11.013.
[29] Abbasi R, Ketabdari MJ. Enhancement of OWC Wells turbine efficiency and performance using riblets covered blades, a numerical study. Energy Convers Manage 2022;254:115212. http://dx.doi.org/10.1016/j.enconman.2022.115212.
[30] Gato LMC, Carrelhas AAD, Cunha AFA. Performance improvement of the axial self-rectifying impulse air-turbine for wave energy conversion by multi-row guide vanes: Design and experimental results. Energy Convers Manage 2021;243:114305. http://dx.doi.org/10.1016/j.enconman.2021.114305.
[31] Otaola E, Garrido AJ, Lekube J, Garrido I. A comparative analysis of self-rectifying turbines for the Mutriku oscillating water column energy plant. Complexity 2019. http://dx.doi.org/10.1155/2019/6396904.
[32] Ozkop E, Altas IH. Control, power and electrical components in wave energy conversion systems: A review of the technologies. Renew Sustain Energy Rev 2017;67:106–15. http://dx.doi.org/10.1016/j.rser.2016.09.012.
[33] Amundarain M, Alberdi M, Garrido AJ, Garrido I, Maseda J. Wave energy plants: Control strategies for avoiding the stalling behaviour in the Wells turbine. Renew Energy 2010;35(12):2639–48. http://dx.doi.org/10.1016/j.renene.2010.04.009.
[34] Alberdi M, Amundarain M, Garrido AJ, Garrido I, Casquero O, De la Sen M. Complementary control of oscillating water column-based wave energy conversion plants to improve the instantaneous power output. IEEE Trans Energy Convers 2011;26(4):1021–32. http://dx.doi.org/10.1109/TEC.2011.2167332.
[35] Das TK, Kerikous E, Venkatesan N, Janiga G, Thévenin D, Samad A. Performance improvement of a Wells turbine through an automated optimization technique. Energy Convers Manag X 2022;16:100285. http://dx.doi.org/10.1016/j.ecmx.2022.100285.
[36] Tedeschi E, Carraro M, Molinas M, Mattavelli P. Effect of control strategies and power take-off efficiency on the power capture from sea waves. IEEE Trans Energy Convers 2011;26(4):1088–98. http://dx.doi.org/10.1109/TEC.2011.2164798.
[37] Song SK, Park JB. Control strategy of an impulse turbine for an oscillating water column wave energy converter in time-domain using Lyapunov stability method. Appl Sci 2016;6(10). http://dx.doi.org/10.3390/app6100281.
[38] Falcão AFO. Control of an oscillating-water-column wave power plant for maximum energy production. Appl Ocean Res 2002;24(2):73–82. http://dx.doi.org/10.1016/S0141-1187(02)00021-4.
[39] Henriques JCC, Portillo JCC, Sheng W, Gato LMC, Falcão AFO. Dynamics and control of air turbines in oscillating-water-column wave energy converters: Analyses and case study. Renew Sustain Energy Rev 2019;112:571–89. http://dx.doi.org/10.1016/j.rser.2019.05.010.
[40] Falcão AFO, Sarmento AJNA, Gato LMC, Brito-Melo A. The Pico OWC wave power plant: Its lifetime from conception to closure 1986 to 2018. Appl Ocean Res 2020;102104. http://dx.doi.org/10.1016/j.apor.2020.102104.
[41] Heath T. Chapter 334 - The development and installation of the Limpet wave energy converter. In: Sayigh A, editor. World renewable energy congress VI. Oxford: Pergamon; 2000, p. 1619–22. http://dx.doi.org/10.1016/B978-008043865-8/50334-2.
[42] Alcorn R, Blavette A, Healy M, Lewis A. FP7 EU funded CORES wave energy project: a coordinators' perspective on the Galway Bay sea trials. Underw Technol 2014. http://dx.doi.org/10.3723/ut.32.051.
[43] Falcão AFO, Henriques JCC. Oscillating-water-column wave energy converters and air turbines: A review. Renew Energy 2016;85:1391–424. http://dx.doi.org/10.1016/j.renene.2015.07.086.
[44] OPERA - Open Sea Operating Experience to Reduce Wave Energy Cost, Contract 654444. 2022, http://opera-h2020.eu/. Accessed April 2022.
[45] Carrelhas AAD, Gato LMC, Henriques JCC, Falcão AFO. Experimental study of a self-rectifying biradial air turbine with fixed guide-vanes arranged into two concentric annular rows. Energy 2020;198:117211. http://dx.doi.org/10.1016/j.energy.2020.117211.
[46] Correia da Fonseca FX, Henriques JCC, Gato LMC, Falcão AFO. Oscillating flow rig for air turbine testing. Renew Energy 2019;142:373–82. http://dx.doi.org/10.1016/j.renene.2019.04.124.
[47] Carrelhas AAD, Gato LMC, Henriques JCC, Falcão AFO, Varandas J. Test results of a 30 kW self-rectifying biradial air turbine-generator prototype. Renew Sustain Energy Rev 2019;109:187–98. http://dx.doi.org/10.1016/j.rser.2019.04.008.
[48] Gato LMC, Henriques JCC, Carrelhas AAD. Sea trial results of the biradial and Wells turbines at Mutriku wave power plant. Energy Convers Manage 2022;268:115936. http://dx.doi.org/10.1016/j.enconman.2022.115936.
[49] IDOM - Consulting, Engineering, Architecture. 2022, https://www.idom.com/. Accessed April 2022.
[50] Faÿ F-X, Henriques JCC, Kelly J, Mueller M, Abusara M, Sheng W, et al. Comparative assessment of control strategies for the biradial turbine in the Mutriku OWC plant. Renew Energy 2020;146:2766–84. http://dx.doi.org/10.1016/j.renene.2019.08.074.
[51] Faÿ F-X, Pujana A, Ruiz-Minguela P, Kelly J, Mueller M, Henriques JCC, et al. Shoreline OWC wave power plant control algorithms. Tech. rep., OPERA - Open Sea Operating Experience to Reduce Wave Energy Costs, Deliverable D4.2; 2018, http://opera-h2020.eu/wp-content/uploads/2018/08/OPERA_D4.2_Shoreline-OWC_wave_power_plant_CL_TECNALIA_2018-08-10_v1.0.pdf.
[52] Gaebele DT, Magaña ME, Brekken TKA, Henriques JCC, Carrelhas AAD, Gato LMC. Second order sliding mode control of oscillating water column wave energy converters for power improvement. IEEE Trans Sustain Energy 2021;12(2):1151–60. http://dx.doi.org/10.1109/TSTE.2020.3035501.
[53] Scialò A, Henriques JCC, Malara G, Falcão AFO, Gato LMC, Arena F. Power take-off selection for a fixed U-OWC wave power plant in the Mediterranean Sea: The case of Roccella Jonica. Energy 2021;215:119085. http://dx.doi.org/10.1016/j.energy.2020.119085.
[54] Henriques JCC, Gato LMC, Falcão AFO, Robles E, Faÿ F-X. Latching control of a floating oscillating-water-column wave energy converter. Renew Energy 2016;90:229–41. http://dx.doi.org/10.1016/j.renene.2015.12.065.
[55] Henriques JCC, Gato LMC, Lemos JM, Gomes RPF, Falcão AFO. Peak-power control of a grid-integrated oscillating water column wave energy converter. Energy 2016;109:378–90. http://dx.doi.org/10.1016/j.energy.2016.04.098.
[56] Henriques JCC, Gomes RPF, Gato LMC, Falcão AFO, Robles E, Ceballos S. Testing and control of a power take-off system for an oscillating-water-column wave energy converter. Renew Energy 2016;85:714–24. http://dx.doi.org/10.1016/j.renene.2015.07.015.
[57] Henriques JCC, Gato LMC, Carrelhas AAD, Varandas J. Open-sea performance and reliability of the OWC turbine and electrical equipment. Tech. rep., OPERA - Open Sea Operating Experience to Reduce Wave Energy Costs, Deliverable D3.4; 2019, URL http://opera-h2020.eu/wp-content/uploads/2019/09/OPERA_D3.4_Open-Sea_PerformanceReliability_IST_20190724_v1.0.pdf.
[58] Henriques JCC, Lemos JM, Eça L, Gato LMC, Falcão AFO. A high-order Discontinuous Galerkin Method with mesh refinement for optimal control. Automatica 2017;85:70–82. http://dx.doi.org/10.1016/j.automatica.2017.07.029.
[59] Mutriku biradial turbine post-processing analisys - OPERA H2020. 2022, https://github.com/joaochenriques/opera-mutriku. Accessed April 2022.
[60] Torre-Enciso Y, Ortubia I, I. López de Aguileta L, Marqués J. Mutriku wave power plant: from the thinking out to the reality. In: Procedings 8th European wave tidal energy conference, Uppsala, Sweden. 2009, p. 319–29.
[61] Gato LMC, Maduro AR, Carrelhas AAD, Henriques JCC, Ferreira DN. Performance improvement of the biradial self-rectifying impulse air turbine for wave energy conversion by multi-row guide vanes: Design and experimental results. Energy 2021;216:119110. http://dx.doi.org/10.1016/j.energy.2020.119110.
[62] Faÿ F-X, Robles E, Marcos M, Aldaiturriaga E, Camacho EF. Sea trial results of a predictive algorithm at the Mutriku Wave power plant and controllers assessment based on a detailed plant model. Renew Energy 2020;146:1725–45. http://dx.doi.org/10.1016/j.renene.2019.07.129.
[63] Dixon SL, Hall CA. Fluid mechanics and thermodynamics of turbomachinery. 7th ed.. Oxford: Butterworth-Heinemann; 2013.
[64] Prediccion de oleaje, nível del mar; Boyas mareografos. Puertos del Estado - Gobierno de España, http://www.puertos.es/es-es/oceanografia/Paginas/portus.aspx/. Accessed April 2022.
[65] Ciappi L, Cheli L, Simonetti I, Bianchini A, Manfrida G, Cappietti L. Wave-to-wire model of an oscillating-water-column wave energy converter and its application to Mediterranean energy hot-spots. Energies 2020;13(21). http://dx.doi.org/10.3390/en13215582.
[66] Suchithra R, Ezhilsabareesh K, Samad A. Development of a reduced order wave to wire model of an OWC wave energy converter for control system analysis. Ocean Eng 2019;172:614–28. http://dx.doi.org/10.1016/j.oceaneng.2018.12.013.
[67] Carrelhas AAD, Gato LMC, Henriques JCC, Falcão AFO. Experimental study of a self-rectifying biradial air turbine with fixed guide-vanes arranged into concentric annular rows. Energy 2020;198:117211. http://dx.doi.org/10.1016/j.energy.2020.117211.
[68] Falcão AFO, Gato LMC, Nunes EPAS. A novel radial self-rectifying air turbine for use in wave energy converters. Part 2. Results from model testing. Renew Energy 2013;53:159–64. http://dx.doi.org/10.1016/j.renene.2012.11.018.
[69] Goldberg DE. Genetic algorithms in search, optimization, and machine learning. Addison-Wesley; 1989.